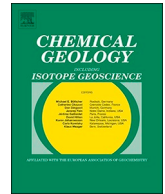




ELSEVIER

Contents lists available at ScienceDirect

Chemical Geology

journal homepage: www.elsevier.com/locate/chemgeo

Coral Li/Mg thermometry: Caveats and constraints

Kristan Cuny-Guirriec^{a,*}, Eric Douville^a, Stéphanie Reynaud^b, Denis Allemand^b, Louise Bordier^a, Marine Canesi^a, Claudio Mazzoli^c, Marco Taviani^{d,e,f}, Simonepietro Canese^g, Malcolm McCulloch^h, Julie Trotterⁱ, Serguei Damián Rico-Esenaro^j, Joan-Albert Sanchez-Cabeza^k, Ana Carolina Ruiz-Fernández^l, Juan P. Carricart-Ganivet^m, Pete M. Scott^h, Aleksey Sadekov^h, Paolo Montagna^{d,n}

^a Laboratoire des Sciences du Climat et de l'Environnement, LSCE/IPSL, CEA-CNRS-UVSQ, Université Paris-Saclay, F-91191 Gif-sur-Yvette, France

^b Centre Scientifique de Monaco, 8 quai Antoine 1er, 98000 Monaco, Monaco

^c Dipartimento di Geoscienze, Università degli Studi di Padova, Via G. Gradenigo 6, 35131 Padova, Italy

^d Institute of Marine Sciences (ISMAR), CNR, Via Gobetti 101, Bologna, Italy

^e Biology Department, Woods Hole Oceanographic Institution, 266 Woods Hole Road, Woods Hole, MA 02543, USA

^f Stazione Zoologica Anton Dohrn, Villa Comunale, 80121 Naples, Italy

^g ISPRA, Via Branconi 48, 00144 Rome, Italy

^h Oceans Graduate School, the UWA Oceans Institute, the ARC Centre of Excellence for Coral Reef Studies, The University of Western Australia, Crawley, Australia

ⁱ School of Earth Sciences, the UWA Oceans Institute, The University of Western Australia, Crawley, Australia

^j Posgrado en Ciencias del Mar y Limnología, Universidad Nacional Autónoma de México, Av. Ciudad Universitaria 3000, C.P. 04510, Coyoacán, Ciudad de México, Mexico

^k Unidad Académica Procesos Oceánicos y Costeros, Instituto de Ciencias del Mar y Limnología, Universidad Nacional Autónoma de México, Ciudad Universitaria, 04510 México, Mexico

^l Unidad Académica Mazatlán, Instituto de Ciencias del Mar y Limnología, Universidad Nacional Autónoma de México, Av. Joel Montes Camarena S/N, 82040 Mazatlán, Mexico

^m Laboratorio de Esclerocronología de Corales Arrecifales, Unidad Académica de Sistemas Arrecifales en Puerto Morelos, Instituto de Ciencias del Mar y Limnología, Universidad Nacional Autónoma de México, ProL. Av. Niños Héroes S/N, Puerto Morelos, Q. Roo 77580, Mexico

ⁿ Lamont-Doherty Earth Observatory, Columbia University, 61 Route 9W, Palisades, NY 10964, USA

ARTICLE INFO

Editor: Michael E. Böttcher

Keywords:

Scleractinian corals

Li/Mg

Paleo-temperature proxy

Organic matter

Calcite contamination

ABSTRACT

The coral Li/Mg temperature proxy is revisited through an in-depth trace element analysis of scleractinians collected live from tropical to polar environments. The dataset consists of Li/Ca, Mg/Ca, Sr/Ca and Li/Mg ratios from 64 coral specimens belonging to 8 different taxa, including both reef-building zooxanthellate and cold-water non-zooxanthellate species, from a wide range of water temperature (−1 to 29.5 °C), salinity (34.71 to 38.61), and depth (3 to 670 m).

Our results showed that the reliability of the Li/Mg temperature proxy is strongly limited by the organic matter associated with the coral skeleton, which is most evident within the green bands observed in tropical corals. Organic-rich bands can double the Mg content otherwise present in the skeleton, which may ultimately lead to a temperature overestimation exceeding 15 °C. We found that this bias can be overcome by the treatment of coral skeletons with a specific oxidizing cleaning protocol. We also detected the presence of calcite deposits within the aragonite skeleton of some Antarctic living coral specimens, which strongly affects the robustness of the Li/Mg proxy given its temperature sensitivity of ~1.5 °C/1% calcite. Therefore, to obtain reliable reconstructions a correction needs to be applied when organic matter and/or calcite contamination is present, which requires the scrupulous assessment of the integrity of the aragonite prior to geochemical analyses. Given that some species entrap more organic matter than others, and that some are more prone to calcite contamination, a taxon-related effect is apparent. Here we show that the tropical species *Porites* spp., *Pseudodiploria strigosa* and *Orbicella annularis*, and the cold-water species *Madrepora oculata*, *Caryophyllia antarctica* and *Flabellum impensum*, are all suitable candidates for reconstructing seawater temperatures.

The integrated results across a wide temperature range, from extreme cold to tropical shallow waters, yield an overall precision for the Li/Mg-temperature proxy of ± 1.0 °C, as quantified by the standard error of estimates. If

* Corresponding author.

E-mail address: kristan.cuny@lscce.ipsl.fr (K. Cuny-Guirriec).

<https://doi.org/10.1016/j.chemgeo.2019.03.038>

Received 22 October 2018; Received in revised form 29 March 2019; Accepted 31 March 2019

Available online 30 April 2019

0009-2541/ © 2019 Published by Elsevier B.V.

calculated from the 95% prediction intervals, the uncertainty of the temperature estimates is $\pm 0.9^\circ\text{C}$ at 1°C , $\pm 1.5^\circ\text{C}$ at 12°C and $\pm 2.6^\circ\text{C}$ at 25°C . However, the uncertainty for the tropical corals (e.g. *Porites*) can be reduced to $\pm 0.6^\circ\text{C}$ if a Li/Mg and Sr/Ca multi-regression approach is applied.

1. Introduction

Earth's ecosystems are increasingly threatened by multiple stressors related to human activities (Ripple et al., 2017). The Intergovernmental Panel on Climate Change has recently warned about the specific threat of CO_2 release and consequent increasing temperatures (Allen et al., in press). This acceleration in global warming has highlighted the need for improved climate projections by examining historical instrument data and reconstructing paleoclimate records from natural archives. Paleoclimate reconstructions can help to overcome the absence of long and continuous instrumental climate records that are needed to evaluate the likely impacts and consequences of climate change and global warming on the environment and ecosystem. It is therefore crucial to develop effective climate proxies to obtain better paleoclimate reconstructions. A number of proxies have been developed to evaluate temperatures in the upper ocean system, which include faunal assemblages (e.g. Mix et al., 1999), alkenones in sediments (e.g. Müller et al., 1998), Mg/Ca (e.g. Dekens et al., 2002) and $\delta^{18}\text{O}$ (e.g. Bemis et al., 1998) in planktonic foraminifera, Sr/Ca and Mg/Ca in tropical corals (e.g. Corrège, 2006; Mitsuguchi et al., 1996), and more recently clumped isotopes (Ghosh et al., 2006). However, relatively few proxies have been developed for deep/cold water environments (Montagna et al., 2014). In general, the effectiveness of geochemical proxies can be compromised by complications induced mainly by the physiology of the organism, and diagenetic processes.

The Li/Mg ratio in aragonite foraminifera and corals was established as a proxy to reconstruct seawater temperatures (Bryan and Marchitto, 2008; Case et al., 2010; Raddatz et al., 2013; Montagna et al., 2014). Its use gained support as it was considered to be only moderately affected by coral physiology or by fine-scale skeletal variations (e.g. centres of calcification vs. fibrous aragonite), and hence largely independent of species controls, so it could be applied across a wide range of environments and species. A general exponential calibration curve showed a direct relationship between coral Li/Mg ratios and ambient seawater temperature, for both cold-water and tropical corals across a temperature range of $0.75\text{--}28^\circ\text{C}$, with an uncertainty in the Li/Mg-derived temperature of $\pm 0.9^\circ\text{C}$ (Hathorne et al., 2013; Montagna et al., 2014). However, some uncertainties remain, such as the mechanisms of Li and Mg incorporation in the skeleton during the bio-mineralization process, the microstructure-related Li/Mg variations, and the mechanisms explaining the ultimate link with temperature (Montagna et al., 2014; Rollion-Bard and Blamart, 2015; Marchitto et al., 2018). More recently, advantages of a multi-proxy approach combining Li/Mg and Sr/Ca have provided more accurate temperature reconstructions by reducing apparent species effects (Fowell et al., 2016; D'Olivo et al., 2018; Zinke et al., 2019).

The present study aims to resolve some of the uncertainties that can affect the reliability of Li/Mg as a temperature proxy in corals. In particular, we discuss the effects of organic matter in the coral skeleton, which is known to alter the coral geochemistry and hence bias climate reconstructions (Boiseau and Juillet-Leclerc, 1997; Mitsuguchi et al., 2001; Watanabe et al., 2001; Barker et al., 2003; Holcomb et al., 2015). Organic matter found in corals may have various origins, including the polyp-derived skeletal organic matrix that is believed to act as a template for initial crystal nucleation (e.g. Cuif et al., 2008; Mass et al., 2013; Takeuchi et al., 2016), the organic membranes of the living polyps, the deposition of bacteria or algal symbionts rich in chlorophyll, and seawater-sourced organic matter entrapped in the coral skeleton (DeCarlo et al., 2018). Although the effect of organic matter on

geochemical proxies, such as Mg/Ca, Sr/Ca, $\delta^{18}\text{O}$ and $\delta^{11}\text{B}$, is relatively well-documented (Mitsuguchi et al., 2001; Watanabe et al., 2001), little is known about its effect on the Li/Ca and Li/Mg ratios (Holcomb et al., 2015). Finally, we discuss the purity of the skeletal aragonite mineralogy, including calcite contamination as a factor influencing the fidelity of the Li/Mg proxy.

The calibration curve of Montagna et al. (2014) is expanded here to include extreme temperatures using new Li/Mg data, from both laser and solution-based ICP-MS analyses of corals from sub-zero temperature waters in Antarctica. We also further evaluate the general link existing between coral Li/Mg and Sr/Ca ratios and the ambient seawater temperature, and the validity of using Li/Mg and Sr/Ca multi-regressions to reduce uncertainties on reconstructed temperatures (Fowell et al., 2016; D'Olivo et al., 2018).

2. Samples and methods

2.1. Coral samples

We investigated 64 scleractinian corals, both zooxanthellate ($n = 47$) and non-zooxanthellate ($n = 17$), collected live from the Mediterranean Sea, Caribbean Sea, Pacific Ocean, and Ross Sea, from waters spanning a wide range in temperature (-1 to 29.5°C), salinity (34.71 to 38.61), and depth (3 to 670 m) (Table 1, Fig. 1). We examined 11 different species of 8 different genera: *Porites* spp., *Orbicella faveolata*, *Orbicella annularis*, *Pseudodiploria strigosa*, *Madrepora oculata*, *Javania antarctica*, *Flabellum impensum*, *Flabellum gardineri*, *Caryophyllia antarctica*, and *Paraconotrochus antarcticus* (Table 1). Seawater temperature data at the sampling locations were obtained from the Advanced Very High Resolution Radiometer Optimum Interpolation Sea Surface Temperature version 2 (AVHRR-OISSTv2, 0.25° grid; Banzon et al., 2016; Reynolds et al., 2007) for shallow-water corals, and from NOAA WOA13v2 (0.25° grid) for specimens living below 10 m depth (Boyer et al., 2013). When available, we used in situ temperature data that had been acquired using CTD (conductivity, temperature, depth) profiles near the coral sampling site (Table 1). Salinity data for all the sampling locations were obtained from the NOAA WOA13v2 dataset. Seawater temperature data from the AVHRR-OISSTv2 database cover the same period corresponding to the coral portion sub-sampled for geochemistry (i.e. the last 4–6 years, see below).

2.1.1. Reef-building zooxanthellate corals

Cores were collected from 10 living *Porites* sp. coral colonies along the intertropical zone of the Pacific Ocean using an underwater hydraulic drill, during the TARA Pacific expedition (2016–2018). These colonies were sampled at various depths, from 3 m at Moorea Island down to 20 m at Wallis Islands, and mean seawater temperatures, from 22.4°C near Easter Island to 29.0°C near Wallis Island. In November 2015, 25 short cores were extracted from *Porites lobata* colonies living in the lagoonal Uitoé and Dumbéa Fausse passe reefs, New Caledonia, between 3 and 51 m, within a temperature range of $22.4\text{--}26.6^\circ\text{C}$. These *P. lobata* colonies were exposed to different levels of sunlight irradiance, with 3 colonies (06, 08 and 28) having portions growing under conditions of variable intensity, from shady to direct sunlight, and two colonies (11.5 and 15.5) growing entirely under shady conditions.

Short cores (~ 10 cm long) were collected in 2017 with a Nemo underwater drill system from 12 living *Orbicella* spp. ($n = 9$) and *P. strigosa* ($n = 3$) coral colonies growing at 5 m water depth, within a few meters long transect, in Puerto Morelos Reef, northeast coast of the

Table 1
Geographic coordinates and depth of the coral sampling locations, with corresponding seawater temperature and salinity values.

Sample code	Sampling location	Latitude	Longitude	Depth (m)	Coral species	Temperature (°C)			Salinity	Source of seawater data
						Annual mean	σ	Winter		
Ross Sea (Antarctica)										
GRC-02-001	Iselin Bank	72°16.11' S	176°36.28' W	670	<i>Javania antarctica</i>	0.93	0.05		34.71	WOA13 v2 (0.25deg)
GRC-02-008					<i>Javania antarctica</i>	0.93	0.05		34.71	
GRC-02-009					<i>Javania antarctica</i>	0.93	0.05		34.71	
GRC-02-010					<i>Javania antarctica</i>	0.93	0.05		34.71	
GRC-02-011					<i>Javania antarctica</i>	0.93	0.05		34.71	
GRC-02-013					<i>Javania antarctica</i>	0.93	0.05		34.71	
GRC-02-020					<i>Javania antarctica</i>	0.93	0.05		34.71	
GRC-02-021					<i>Javania antarctica</i>	0.93	0.05		34.71	
GRC-02-002					<i>Flabellum impensum</i>	0.93	0.05		34.71	
GRC-02-056					<i>Flabellum gardineri</i>	0.93	0.05		34.71	
GRC-02-014					<i>Paraconotochus antarcticus</i>	0.93	0.05		34.71	
GRC-02-015					<i>Paraconotochus antarcticus</i>	0.93	0.05		34.71	
GRC-02-050					<i>Paraconotochus antarcticus</i>	0.93	0.05		34.71	
GRC-02-003					<i>Caryophyllia antarctica</i>	0.93	0.05		34.71	
GRC-02-024	<i>Caryophyllia antarctica</i>	0.93	0.05		34.71					
CARBONANT34	Mawson Bank	73°14.56' S	175°38.35' E	389	<i>Flabellum impensum</i>	-0.76	0.05		34.70	
Mediterranean Sea										
Records 21-6	Sardinia Channel	38°42.197' N	8°54.735' E	432	<i>Madrepora oculata</i>	13.80	0.10		38.61	in-situ and WOA13 v2 (0.25deg)
Caribbean Sea										
MEX 01	Puerto Morelos	20°52.739' N	86°50.949' W	5	<i>Orbicella faveolata</i>	27.9	1.1	29.3	35.98	AVHRR-OISST v2
MEX 02					<i>Orbicella faveolata</i>	27.9	1.1	29.3	35.98	
MEX 02-Wall					<i>Orbicella faveolata</i>	27.9	1.1	29.3	35.98	
MEX 05					<i>Orbicella faveolata</i>	27.9	1.1	29.3	35.98	
MEX 05-Wall					<i>Orbicella faveolata</i>	27.9	1.1	29.3	35.98	
MEX 06					<i>Orbicella faveolata</i>	27.9	1.1	29.3	35.98	
MEX 06-Wall					<i>Orbicella faveolata</i>	27.9	1.1	29.3	35.98	
MEX 10					<i>Orbicella faveolata</i>	27.9	1.1	29.3	35.98	
MEX 11					<i>Orbicella faveolata</i>	27.9	1.1	29.3	35.98	
MEX 12					<i>Orbicella faveolata</i>	27.9	1.1	29.3	35.98	
MEX 13					<i>Orbicella faveolata</i>	27.9	1.1	29.3	35.98	
MEX 09					<i>Orbicella annularis</i>	27.9	1.1	29.3	35.98	
MEX 03					<i>Pseudodiploria strigosa</i>	27.9	1.1	29.3	35.98	
MEX 03-Wall					<i>Pseudodiploria strigosa</i>	27.9	1.1	29.3	35.98	
MEX 04					<i>Pseudodiploria strigosa</i>	27.9	1.1	29.3	35.98	
MEX 04-Wall	<i>Pseudodiploria strigosa</i>	27.9	1.1	29.3	35.98					
MEX 15	<i>Pseudodiploria strigosa</i>	27.9	1.1	29.3	35.98					

(continued on next page)

Table 1 (continued)

Sample code	Sampling location	Latitude	Longitude	Depth (m)	Coral species	Temperature (°C)			Salinity	Source of seawater data
						Annual mean	σ	Winter		
New Caledonia										
03.P	Dumbea Fausse passe	22°19.656' S	166°13.220'E	3	<i>Porites lobata</i>	24.6	1.6	26.6	35.42	WOA13 v2 (0.25deg)
06.N-Shadow	Dumbea Fausse passe	22°19.656' S	166°13.220'E	6	<i>Porites lobata</i>	24.6	1.6	26.6	35.42	
06.O	Dumbea Fausse passe	22°19.656' S	166°13.220'E	6	<i>Porites lobata</i>	24.6	1.6	26.6	35.42	
08.L-Shadow	Dumbea Fausse passe	22°19.656' S	166°13.220'E	8	<i>Porites lobata</i>	24.6	1.6	26.6	35.43	
08.M	Dumbea Fausse passe	22°19.656' S	166°13.220'E	8	<i>Porites lobata</i>	24.6	1.6	26.6	35.43	
09.K	Dumbea Fausse passe	22°19.656' S	166°13.220'E	9	<i>Porites lobata</i>	24.6	1.6	26.6	35.44	
11.5-8-Shadow	Uitoe Fausse passe	22°17.033' S	166°10.882' E	11.5	<i>Porites lobata</i>	24.5	1.6	26.5	35.44	
12.5.J	Dumbea Fausse passe	22°19.656' S	166°13.220'E	12.5	<i>Porites lobata</i>	24.6	1.6	26.5	35.44	
13.6	Uitoe Fausse passe	22°17.033' S	166°10.882' E	13.6	<i>Porites lobata</i>	24.5	1.6	26.5	35.44	
15.5-Shadow	Uitoe Fausse passe	22°17.033' S	166°10.882' E	15.5	<i>Porites lobata</i>	24.5	1.6	26.5	35.44	
16.4	Uitoe Fausse passe	22°17.033' S	166°10.882' E	16.4	<i>Porites lobata</i>	24.5	1.6	26.5	35.44	
18.1	Dumbea Fausse passe	22°19.656' S	166°13.220'E	18.1	<i>Porites lobata</i>	24.5	1.6	26.4	35.44	
18.5	Uitoe Fausse passe	22°17.033' S	166°10.882' E	18.5	<i>Porites lobata</i>	24.5	1.6	26.4	35.44	
21.3	Uitoe Fausse passe	22°17.033' S	166°10.882' E	21.3	<i>Porites lobata</i>	24.4	1.6	26.4	35.45	
23.H	Dumbea Fausse passe	22°19.656' S	166°13.220'E	23	<i>Porites lobata</i>	24.4	1.6	26.3	35.45	
24.9	Uitoe Fausse passe	22°17.033' S	166°10.882' E	24.9	<i>Porites lobata</i>	24.4	1.6	26.3	35.46	
27.2	Uitoe Fausse passe	22°17.033' S	166°10.882' E	27.2	<i>Porites lobata</i>	24.4	1.6	26.2	35.46	
28.F-Shadow	Dumbea Fausse passe	22°19.656' S	166°13.220'E	28	<i>Porites lobata</i>	24.3	1.6	26.2	35.46	
28.G	Dumbea Fausse passe	22°19.656' S	166°13.220'E	28	<i>Porites lobata</i>	24.3	1.6	26.2	35.46	
35	Uitoe Fausse passe	22°17.033' S	166°10.882' E	35	<i>Porites lobata</i>	24.2	1.6	25.9	35.48	
35.E	Dumbea Fausse passe	22°19.656' S	166°13.220'E	35	<i>Porites lobata</i>	24.2	1.6	25.9	35.48	
38.D	Dumbea Fausse passe	22°19.656' S	166°13.220'E	38	<i>Porites lobata</i>	24.1	1.6	25.8	35.48	
44.C	Dumbea Fausse passe	22°19.656' S	166°13.220'E	44	<i>Porites lobata</i>	24.0	1.6	25.5	35.49	
45.1	Uitoe Fausse passe	22°17.033' S	166°10.882' E	45.1	<i>Porites lobata</i>	24.0	1.6	25.4	35.50	
51.B	Dumbea Fausse passe	22°19.656' S	166°13.220'E	51	<i>Porites lobata</i>	23.8	1.6	25.1	35.51	
Pacific Ocean										
TARA-P I2S3c21	Panama	7°12.3312' N	81°47.4632' W	8	<i>Porites</i> sp.	28.6	0.6	29.2	31.81	AVHRR-OISST v2
TARA-P I4S1	Easter Island	27°04.76008' S	109°19.24060' W	14	<i>Porites</i> sp.	22.4	1.6	25.3	36.04	
TARA-P I5S4	Easter Island	27°04.76008' S	109°19.24060' W	14	<i>Porites</i> sp.	22.4	1.6	25.3	36.05	
TARA-P I6S2	Gambier Island	23°09.54378' S	134°50.53520' W	9	<i>Porites</i> sp.	25.2	1.3	27.5	36.08	
TARA-P I7S1c1	Moorea Island	17°28.560' S	149°48.675' W	3	<i>Porites</i> sp.	27.8	0.7	28.9	35.91	
TARA-P I7S3c2	Moorea Island	17°29.380' S	149°45.303' W	13	<i>Porites</i> sp.	27.8	0.7	28.9	35.91	
TARA-P I8S1c3	Aitutaki (Cook Islands)	18°50.406' S	159°48.054' W	14	<i>Porites</i> sp.	27.1	0.8	28.4	35.67	
TARA-P II10S0c6	Samoa Islands	13°50.879' S	172°04.424' W	9	<i>Porites</i> sp.	28.9	0.4	29.6	35.17	
TARA-P II11S1c7	Wallis Island	13°18.00' S	176°12.00' W	20	<i>Porites</i> sp.	29.0	0.5	29.6	35.06	
TARA-P II15S1c10	Guam Island	13°14.984' N	144°38.697' E	9	<i>Porites</i> sp.	28.9	0.4	29.6	35.39	

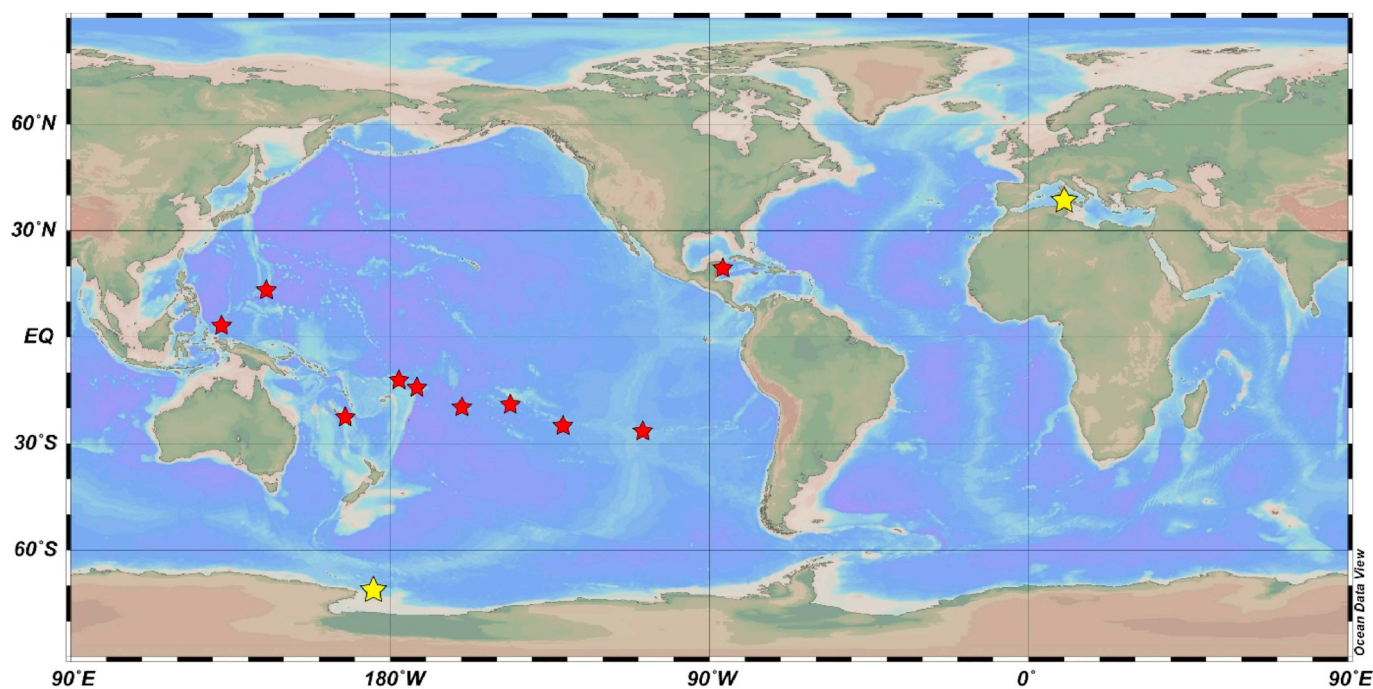


Fig. 1. Sampling locations of coral colonies. Red stars: zooxanthellate corals; yellow stars: non-zooxanthellate corals. (For interpretation of the references to colour in this figure legend, the reader is referred to the web version of this article.)

Yucatán Peninsula, Mexico (Fig. 1). The average SST at the sampling site was 27.9 °C, and temperatures ranged between 26.4 °C in winter and 29.3 °C in summer (Table 1).

The *Porites* spp., *Orbicella* spp., and *P. strigosa* cores were imaged using a DISCOVERY CT750 HD computerized tomography scanner with 0.62 mm resolution, to identify high and low density growth bands. Scans were conducted at Platform DOSEO, CEA-Paris-Saclay. The cores were then cut along the major growth axis with a rock saw and the skeletal portion corresponding to the last 4–6 years (2010–2016), based on density banding, was sub-sampled for trace element analysis using a fine diamond saw. In addition, skeletal aragonite was collected along the thecal wall of four *O. faveolata* and two *P. strigosa* cores using a small diamond bur, carefully avoiding extrathecal material (Table 1).

2.1.2. Cold-water non-zooxanthellate corals

A small living colony of the framework-forming cold-water coral, *Madrepora oculata*, was collected from the Sardinia Channel (Mediterranean Sea) at 432 m water depth using a Remotely Operated Vehicle on the R/V *Urania* during the RECORD 2014 cruise (Taviani et al., 2017). The seawater temperature was obtained from a CTD profile acquired close to the sampling location and was compared to the value sourced from the WOA13v2 dataset to obtain the long-term temperature variability (13.8 ± 0.1 °C). The topmost portion of one of the branches, corresponding to ~1 year of skeletal growth (Orejas et al., 2011), was carefully cleaned using a fine diamond saw to remove any organic material residues, and sub-sampled in 6 different aliquots of ~50 mg each. The other living non-zooxanthellate corals investigated in this study were collected from the Ross Sea (Antarctica) at 389 and 670 m water depth during the XVII (2002) and XXXII (2017) Antarctic campaigns aboard the R/V *Italica* and include 5 different species: *Javania antarctica*, *Caryophyllia antarctica*, *Flabellum impensum*, *Flabellum gardineri* and *Paraconotrachus antarcticus*. The temperatures at the sampling sites are -0.76 ± 0.05 °C and 0.93 ± 0.05 °C. The topmost portion of the skeleton of each specimen, corresponding to ~5–10 years of growth based on growth estimates (Henry and Torres, 2013; Fallon et al., 2014), was sub-sampled and carefully cleaned using a diamond dental disc.

Each of the skeletal portions extracted from the zooxanthellate and

non-zooxanthellate coral samples was finely crushed in an agate mortar, thoroughly mixed, and separated into two aliquots of ~50–100 mg that were transferred to acid-cleaned vials. An aliquot of each sample was cleaned through an oxidative cleaning step (Section 2.2.) before being dissolved and analysed for trace elements. The remaining aliquots of the Caribbean Sea and New Caledonia samples were rinsed with MilliQ water (18Ω) and dissolved in 0.5 N HNO₃. The comparison between “cleaned” and “uncleaned” aliquots allowed us to evaluate the potential effects of organic contamination on the trace element compositions, and specifically on the Li/Mg temperature proxy.

2.2. Chemical treatment

Most trace elements measured in coral skeletons commonly used as proxies for climate reconstructions are biased by the presence of organic matter embedded in the carbonate matrix, or adsorbed on the skeletal surface (Amiel et al., 1973a, 1973b; Allison, 1996). In addition, high concentrations of chlorophyll, associated with the endolithic algae of the genus *Ostreobium* (Le Campion-Alsumard et al., 1995; Massé et al., 2018), may also affect geochemical signals. However, the impact of chlorophyll on the Li/Mg temperature proxy has not yet been quantified. In this study, different cleaning protocols were tested in order to remove Mg and Li associated with organic contamination and surface adsorption, without removing the fraction incorporated into the coral aragonite matrix (Mitsuguchi et al., 2001; Watanabe et al., 2001). The cleaning protocols were tested on two samples of *O. faveolata* collected live from Puerto Morelos, one characterized by green bands (2–5 mm thick, mainly developed at ~1.5 cm from the surface) indicating the presence of *Ostreobium* algae (“contaminated” sample), and the other “clean” sample with no apparent green band was used as a control. In parallel, we applied the same cleaning protocols on an in-house *Porites* standard (M1P-p) to assess the possible alteration of the initial elemental composition of the skeleton. Samples were finely crushed and split into 5 groups, each consisting of 3 subsamples of ~60 mg transferred to acid-cleaned vials. All groups were cleaned with MilliQ water in an ultrasonic bath for 30s, repeated twice (protocol 1). Subsequently, groups 2, 3, 4 and 5 underwent specific chemical

treatments: group 2 was cleaned with a mixture of 1% H₂O₂ buffered with 0.1 M NH₄OH (protocol 2a); group 3 with a mixture of 5% H₂O₂ buffered with 0.2 M NH₄OH (protocol 2b); group 4 with a mixture of 15% H₂O₂ buffered with 0.5 M NH₄OH (protocol 2c); and group 5 was treated with 5% NaOCl solution in an ultrasonic bath for 5 min, then rinsed with MilliQ water several times (protocol 3). During treatments, groups 2, 3 and 4 were placed in a water bath at 60 °C for 20 min and then rinsed with MilliQ several times. Between each step, vials containing the powder and the cleaning solution were centrifuged at 2320 G for 3 min and the supernatant discarded. After cleaning treatments, samples were dried at 40 °C and dissolved in 0.5 N HNO₃ to obtain 100 ppm Ca solutions that were analysed by ICP-MS (Section 2.3). Based on the Li/Ca, Mg/Ca and Li/Mg results (Section 3), we decided to apply the cleaning protocol 2c to all the other samples.

2.3. Analytical methods

2.3.1. Solution quadrupole ICP-MS

Cleaned coral samples were dissolved in 0.5 N HNO₃ (Optima Fisher Ultra Trace Element Analysis, 67%) and analysed using a Quadrupole ICP-MS X-Series II at LSCE (Gif-sur-Yvette, France). ⁷Li, ²⁴Mg, ^{43,44}Ca, ^{86,87,88}Sr, and ²³⁸U isotopes were selected to quantify their elemental concentration in the skeleton following Montagna et al. (2014). Briefly, elemental analysis was performed through a standard addition protocol, using commercial SCP Sciences mono- or multi-standards Inorganic Venture solutions; all standard and sample solutions were diluted to obtain 100 ppm Ca concentration. Data quality was controlled by the analysis of five external carbonate standards (Aragonite AK, RS3, coral JCp1, clam JcT-1 and M1P-p). Replicate analyses of the standards were made after 5 or 10 samples to correct for instrumental drift. Typical mean values and external reproducibility (1σ RSD) obtained by multiple analyses ($n = 13$) of M1P-p during several analytical sequences were: Li/Ca = 6.05 μmol/mol ($\pm 1.17\%$), Mg/Ca = 4.35 mmol/mol ($\pm 0.52\%$), Sr/Ca = 9.02 mmol/mol ($\pm 0.44\%$), U/Ca = 1.10 μmol/mol ($\pm 1.00\%$) and Li/Mg = 1.39 mmol/mol ($\pm 0.68\%$). The reproducibility was improved by a factor of 2 compared to the protocol described by Montagna et al. (2014), thus reducing the uncertainties from quadrupole ICP-MS measurements in the Li/Mg temperature calculations. This improvement resulted from a better control of the memory effect and blank contribution by limiting the Li concentration to 100 ppb for the most enriched standard solution. In addition, the acquisition statistic and the reading time of the Li and Mg signals were substantially increased by doubling the number of sweeps and limiting the number of isotopes analysed. Finally, sample solutions were systematically bracketed by the analysis of blanks every five or ten samples (not every sample), increasing the stability of the analytical sequences.

2.3.2. Laser ablation ICP-MS

Four cold-water coral samples from the Ross Sea were also analysed by laser ablation ICP-MS to investigate micro-scale geochemical variations related to coral microstructures (centres of calcification vs. fibrous aragonite) or the presence of mineralogical phases other than aragonite. The topmost portion of the samples was embedded in epoxy resin, glued to a glass slide and lapped to a final thickness between 50 and 100 μm. The thin sections were analysed using a 193 nm ArF excimer laser system (Teledyne® G2) connected to a SF-ICP-MS (Thermo Scientific™ Element XR) at the University of Western Australia. The isotopes ⁷Li, ²⁵Mg, ⁴³Ca, ⁸⁶Sr and ²³⁸U were selected for analysis and calibrated with the standard JCp-1, which was analysed as a recrystallized powder pellet showing identical values to those from solution-based analysis (Sadekov et al., 2019). External reproducibility (1σ RSD) assessed by analysing the JCp-1 standard was 14.6% for Li/Ca, 5.7% for Mg/Ca and 14.4% for Li/Mg. Analyses were conducted on different skeletal portions using a 80 μm spot at 8 Hz with a laser fluence of 4 J/cm², and a dwell time of 30 ms. Data processing and outlier rejection follows

Langer et al. (2015).

2.3.3. XRD and mRaman spectroscopy

X-ray powder diffraction (XRD) analyses were performed on five Antarctic samples at the Center of Analyses and Services for Certification (CEASC) of the University of Padova using a PANalytical X'Pert 3 Powder diffractometer (Bragg Brentano θ - θ geometry) equipped with Cu X-ray tube, operating at 40 kV and 40 mA, sample spinner, BBHD mirror and solid-state detector (PixCel). Powdered samples were evenly spread on a silicon zero background sample holder. Scans were performed over the range 3 to 80° 2 θ with a virtual step size of 0.017° 2 θ and counting times of 100 s per step. The software program High Score Plus 4 (PANalytical) was used for phase identification and quantitative phase analysis with Rietveld refinement. Refined parameters were: (i) scale factors; (ii) zero-shift; (iii) background; (iv) lattice constant; (v) profile parameters (Gaussian and Lorentzian coefficients). The detection limit for the majority of the mineral phases is around 1%.

Samples GRC-02-014 (*P. antarcticus*) and GRC-02-056 (*F. gardineri*) were also analysed using mRaman spectroscopy. Aragonite and calcite were discriminated, and their spatial distribution mapped for the different L (libration lattice mode) peak in their Raman spectra, which is located at about 206 cm⁻¹ and 282 cm⁻¹, respectively. Spectra were recorded in the frequency range 100–3500 cm⁻¹ using a Thermo Scientific™ DXR™ Raman Microscope with a 780 nm, a 50× long working distance (LWD) objective, at ~5 mW of power and a 25 μm pinhole, obtaining ~2.5 cm⁻¹ spectral resolution and 1.1 μm spatial resolution. To optimize the signal to noise ratio, 6 scans of 30 s were acquired per spectrum.

3. Results

3.1. Chemical treatment

Fig. 2 and Table S1 show the results of the different cleaning protocols applied to the two *O. faveolata* samples from Puerto Morelos, one “contaminated” by organic matter rich bands (Fig. 3), and another “clean” without a green band used as control sample. The average Mg/Ca ratio of the sub-samples that were treated only with MilliQ water is particularly high for the sample with the green band (7.32 ± 0.14 mmol/mol) compared to the control sample (4.26 ± 0.01 mmol/mol), and significantly affects the Li/Mg ratio.

The application of the four treatments (2a, 2b, 2c and 3) effectively reduced the Mg/Ca ratio by 20 to 35% in the “contaminated” sample but did not alter the skeletal composition of the M1P-p *Porites* standard (< 1%) and only slightly that of the “clean” *O. faveolata* specimen (< 4%) (Table S1). The Li/Ca ratio decreased by ~7%, ~6% and < 1% in the “contaminated”, “clean” and M1P-p standard, respectively. The decrease in Mg/Ca and Li/Ca ratios in the “clean” sample might be due to the presence of organic material residues that are not visible. The most appropriate cleaning protocol was selected based on the largest decrease in Mg/Ca ratio and the lowest inter-samples variability in the “contaminated” sample. Accordingly, protocol 2c, with samples treated with 15% H₂O₂ buffered with 0.5 M NH₄OH, seems the most efficient and was systematically adopted to clean all the other coral samples (Fig. 2).

3.2. Zooxanthellate corals

3.2.1. *Porites* spp.

The 25 samples of *P. lobata* from New Caledonia lagoon yielded Li/Ca, Mg/Ca and Li/Mg ratios ranging from 6.07 to 7.43 μmol/mol, 3.52 to 4.33 mmol/mol, and 1.57 to 1.84 mmol/mol, respectively (Table 2). The oxidative cleaning did not significantly affect Me/Ca ratios for those samples, resulting in a mean Li/Ca, Mg/Ca and Li/Mg decrease of 1.5, 0.7 and 0.9%, respectively. The Li/Mg-derived temperatures are

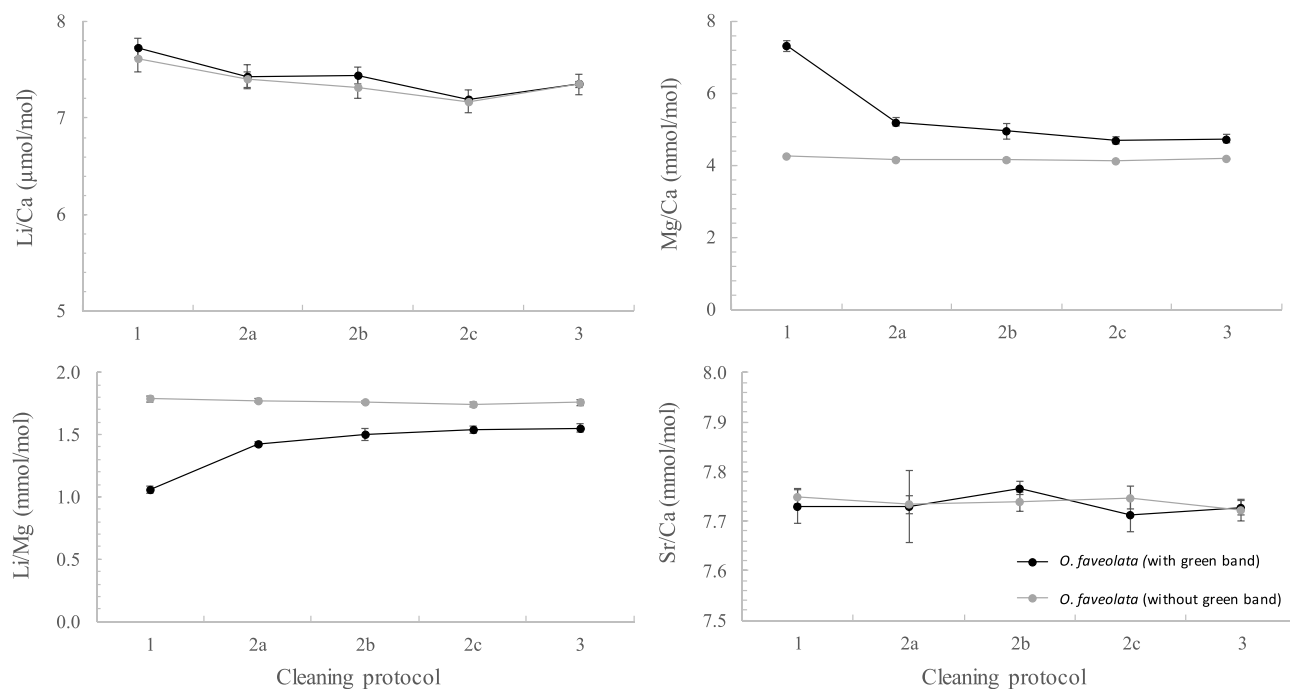


Fig. 2. Li/Ca, Mg/Ca, Li/Mg and Sr/Ca ratios obtained from *O. faveolata* samples as a function of different cleaning protocol tests (1: MilliQ water rinse; 2a: 1% H₂O₂ + 0.1 M NH₄OH; 2b: 5% H₂O₂ + 0.2 M NH₄OH; 2c: 15% H₂O₂ + 0.5 M NH₄OH; 3: 5% NaOCl). The contaminated sample (black dots) was characterized by a distinct green band indicating the presence of *Ostreobium* algae, whereas the control sample (grey dots) did not show any visible green band. Each value is the average ($\pm 1\sigma$ SD) of 3 subsamples of coral powder (see table S1).

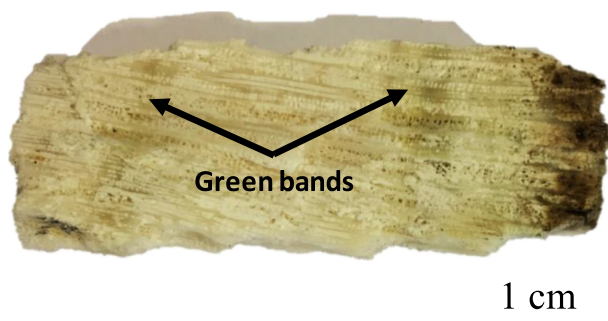


Fig. 3. Picture of the MEX 05 *Orbicella faveolata* sample with well-evident greenish bands on the skeleton surface, associated with organic matter incorporation.

consistent with surface seawater temperature, but underestimate deeper waters temperatures (up to -2°C at 44 m) (Fig. 4). Nevertheless, the application of the cleaning protocol 2c led to slight reductions in the reconstructed temperatures between uncleaned ($\Delta T = -2.4$ to 0.5°C) and cleaned ($\Delta T = -2.0$ to 0.6°C) samples, where ΔT represents the shift between ambient seawater temperature and Li/Mg-reconstructed temperature, using exponential equation described by Montagna et al. (2014).

The cleaned *Porites* spp. samples from the TARA Pacific expedition show a larger geochemical variability compared to cleaned specimens from New Caledonia, with Li/Ca, Mg/Ca and Li/Mg ranging from 5.58 to 6.92 $\mu\text{mol/mol}$, 3.60 to 5.30 mmol/mol, and 1.18 to 1.92 mmol/mol respectively. These ranges are similar to those found in *Porites* from Ogasawara Island in Japan and Tahiti (Hathorne et al., 2013), and in the tropical Pacific (Montagna et al., 2014). However, they differ from the *Porites* samples analysed by Rollion-Bard and Blamart (2015) that are characterized by higher Li/Ca (6.1 to 21.6 $\mu\text{mol/mol}$) and Mg/Ca (3.05 to 8.10 mmol/mol), which they relate to the possible influence of centres of calcification (COC) enriched in both ratios. The Li/Mg-

derived temperatures from the TARA samples generally agree with ambient seawater values, with most of the reconstructed temperatures deviating by < 1 – 1.5°C (Table 2). However, three samples display larger variations ($\geq 2^{\circ}\text{C}$).

3.2.2. *Orbicella* spp. and *P. strigosa*

The cleaned *Orbicella* spp. samples from the Mexican Caribbean show smaller Li/Mg variability (0.53 mmol/mol) than *Porites* spp. (0.75 mmol/mol). Variability is largely controlled by the Mg/Ca contents (4.04 to 5.89 mmol/mol), as Li/Ca ratios are rather stable (6.28 to 6.72 $\mu\text{mol/mol}$).

The Mg/Ca and Li/Ca ratios of the *P. strigosa* samples (Mg/Ca: 3.68 to 4.55 mmol/mol; Li/Ca: 5.91 to 6.44 $\mu\text{mol/mol}$) are lower than values in *Orbicella* spp., and the Li/Mg ratios show lower variability (0.19 mmol/mol).

The oxidative cleaning of the Mexican coral species had a strong impact on trace elements. The mean loss of Mg/Ca for *Orbicella* spp. was up to 25%, while Li was less affected by cleaning ($< 1\%$ of loss), resulting in a mean Li/Mg enrichment of $\sim 26\%$. For *P. strigosa*, the mean Mg/Ca loss was $< 4\%$, leading to a Li/Mg enrichment of $\sim 3\%$ (Table 2, Table S2). The influence of organic matter related to the green band on the Li/Mg-derived temperatures is clearly detectable. The cleaning protocol induces a strong decrease in Mg/Ca that leads to more realistic temperature estimates, and reduces the difference between the reconstructed and in situ temperatures (Table 2).

3.3. Non-zooxanthellate corals

3.3.1. *Javania antarctica*

The *J. antarctica* samples show Li/Ca, Mg/Ca and Li/Mg ratios ranging from 15.11 to 16.22 $\mu\text{mol/mol}$, 2.66 to 3.62 mmol/mol, and 4.48 to 5.95 mmol/mol, respectively. As for *Orbicella* spp., the larger variability is observed for Mg/Ca (11%, 1σ RSD), while Li/Ca is relatively stable (2%, 1σ RSD). The difference between Li/Mg-derived and ambient temperatures varies from -2.9 to 2.9°C (Table 2). XRD analyses of *J. antarctica* sample GRC-02-001 revealed it has a pristine

Table 2

Li/Ca, Mg/Ca, Li/Mg and Sr/Ca values of zooxanthellate and non-zooxanthellate corals based on solution ICP-MS analysis. Li/Mg-derived temperatures are calculated using Montagna et al. (2014) equation. $T_{\text{rec}} - T_{\text{in-situ}}$ is the difference between the reconstructed and the instrumental temperature.

Sample code	Species	Li/Ca	Mg/Ca	Li/Mg	Sr/Ca	Li/Mg-derived	$T_{\text{rec}} - T_{\text{in-situ}}$
		($\mu\text{mol/mol}$)	(mmol/mol)	(mmol/mol)	(mmol/mol)	T ($^{\circ}\text{C}$)	($^{\circ}\text{C}$)
Ross Sea (Antarctica)							
GRC-02-001	<i>Javania antarctica</i>	15.11	3.06	4.93	11.10	1.9	1.0
GRC-02-008	<i>Javania antarctica</i>	15.98	2.72	5.87	11.33	-1.7	-2.6
GRC-02-009	<i>Javania antarctica</i>	16.22	3.62	4.48	11.17	3.8	2.9
GRC-02-010	<i>Javania antarctica</i>	16.09	2.95	5.46	11.43	-0.2	-1.1
GRC-02-011	<i>Javania antarctica</i>	15.81	3.35	4.72	11.49	2.8	1.9
GRC-02-013	<i>Javania antarctica</i>	15.8	2.77	5.71	11.66	-1.1	-2.0
GRC-02-020	<i>Javania antarctica</i>	15.84	2.66	5.95	11.76	-1.9	-2.9
GRC-02-021	<i>Javania antarctica</i>	15.48	2.87	5.39	11.76	0.1	-0.9
GRC-02-002	<i>Flabellum impensum</i>	12.95	2.59	5.00	10.90	1.6	0.7
GRC-02-056	<i>Flabellum gardineri</i>	25.04	17.45	1.43	10.52	27.1	26.2
GRC-02-014	<i>Paraconotrochus antarcticus</i>	19.40	7.49	2.59	10.59	15.0	14.1
GRC-02-015	<i>Paraconotrochus antarcticus</i>	15.14	3.34	4.54	11.07	3.6	2.7
GRC-02-050	<i>Paraconotrochus antarcticus</i>	19.22	4.29	4.48	10.59	3.8	2.9
GRC-02-003	<i>Caryophyllia antarctica</i>	9.95	2.00	4.98	10.43	1.7	0.7
GRC-02-024	<i>Caryophyllia antarctica</i>	12.98	2.65	4.89	10.72	2.0	1.1
CARBONANT34	<i>Flabellum impensum</i>	12.7	2.29	5.55	11.01	-0.5	0.3
Mediterranean Sea							
Records 21-6	<i>Madrepora oculata</i>	10.72 (0.10)	3.81 (0.09)	2.82 (0.05)	10.09 (0.02)	13.3	-0.4
Caribbean Sea							
MEX 01	<i>Orbicella faveolata</i>	6.56	4.42	1.48	9.31	26.4	-1.5
MEX 01-Wall	<i>Orbicella faveolata</i>	6.72	4.55	1.48	9.20	26.5	-1.4
MEX 02	<i>Orbicella faveolata</i>	6.61	4.61	1.43	9.26	27.1	-0.8
MEX 02-Wall	<i>Orbicella faveolata</i>	6.57	4.89	1.34	9.29	28.4	0.6
MEX 05	<i>Orbicella faveolata</i>	6.49	5.89	1.10	9.30	32.5	4.6
MEX 05-Wall	<i>Orbicella faveolata</i>	6.36	5.87	1.08	9.35	32.8	4.9
MEX 06	<i>Orbicella faveolata</i>	6.59	4.09	1.61	9.33	24.7	-3.1
MEX 06-Wall	<i>Orbicella faveolata</i>	6.51	4.10	1.59	9.34	25.0	-2.9
MEX 10	<i>Orbicella faveolata</i>	6.39	4.04	1.58	9.37	25.1	-2.8
MEX 11	<i>Orbicella faveolata</i>	6.45	4.23	1.52	9.37	25.9	-2.0
MEX 12	<i>Orbicella faveolata</i>	6.28	4.36	1.44	9.03	27.0	-0.9
MEX 13	<i>Orbicella faveolata</i>	6.41	5.83	1.10	9.37	32.5	4.6
MEX 09	<i>Orbicella annularis</i>	6.65	4.76	1.40	9.03	27.6	-0.2
MEX 03	<i>Pseudodiploria strigosa</i>	5.95	3.89	1.53	9.18	25.8	-2.1
MEX 03-Wall	<i>Pseudodiploria strigosa</i>	6.26	4.41	1.42	9.06	27.3	-0.6
MEX 04	<i>Pseudodiploria strigosa</i>	6.16	4.07	1.51	9.11	26.0	-1.9
MEX 04-Wall	<i>Pseudodiploria strigosa</i>	6.44	4.55	1.42	9.07	27.4	-0.5
MEX 15	<i>Pseudodiploria strigosa</i>	5.91	3.68	1.61	9.16	24.8	-3.1
New Caledonia							
03.P	<i>Porites lobata</i>	6.36	4.04	1.57	9.21	25.2	0.6
06.N-Shadow	<i>Porites lobata</i>	6.67	4.03	1.65	9.14	24.2	-0.4
06.O	<i>Porites lobata</i>	6.45	4.09	1.58	9.18	25.2	0.6
08.L-Shadow	<i>Porites lobata</i>	6.47	3.86	1.68	9.15	23.9	-0.7
08.M	<i>Porites lobata</i>	6.49	3.93	1.65	9.16	24.2	-0.3
09.K	<i>Porites lobata</i>	6.40	4.00	1.60	9.16	24.8	0.3
11.5.8-Shadow	<i>Porites lobata</i>	6.07	3.59	1.69	9.22	23.8	-0.8
12.5.J	<i>Porites lobata</i>	6.86	4.18	1.64	9.25	24.4	-0.2
13.6	<i>Porites lobata</i>	6.50	3.77	1.72	9.26	23.3	-1.2
15.5-Shadow	<i>Porites lobata</i>	6.38	3.64	1.75	9.23	23.0	-1.5
16.4	<i>Porites lobata</i>	7.43	4.33	1.72	9.30	23.4	-1.1
18.I	<i>Porites lobata</i>	6.84	4.09	1.67	9.24	24.0	-0.5
18.5	<i>Porites lobata</i>	6.29	3.82	1.65	9.18	24.3	-0.2
21.3	<i>Porites lobata</i>	6.85	4.28	1.60	9.15	24.9	0.4
23.H	<i>Porites lobata</i>	6.64	4.00	1.66	9.18	24.1	-0.3
24.9	<i>Porites lobata</i>	6.42	3.73	1.72	9.24	23.4	-1.0
27.2	<i>Porites lobata</i>	6.85	4.04	1.69	9.23	23.7	-0.7
28.F-Shadow	<i>Porites lobata</i>	6.30	3.85	1.64	9.10	24.4	0.1
28.G	<i>Porites lobata</i>	6.49	3.87	1.68	9.23	23.9	-0.4
35	<i>Porites lobata</i>	7.11	3.94	1.81	9.32	22.4	-1.8
35.E	<i>Porites lobata</i>	6.63	3.81	1.74	9.35	23.1	-1.1
38.D	<i>Porites lobata</i>	6.62	3.67	1.80	9.32	22.4	-1.7
44.C	<i>Porites lobata</i>	6.47	3.52	1.84	9.44	22.0	-2.0
45.1	<i>Porites lobata</i>	7.14	3.96	1.80	9.36	22.4	-1.5
51.B	<i>Porites lobata</i>	6.67	3.63	1.84	9.15	22.0	-1.8
Pacific Ocean							
Tara P 12S3c21	<i>Porites</i> sp.	5.74	4.21	1.36	9.08	28.1	-0.4
Tara P 14S1	<i>Porites</i> sp.	6.83	3.79	1.80	9.36	22.4	0.0
Tara P 15S4	<i>Porites</i> sp.	6.91	3.60	1.92	9.43	21.1	-1.3
Tara P 16S2	<i>Porites</i> sp.	6.92	4.92	1.41	9.02	27.5	2.3

(continued on next page)

Table 2 (continued)

Sample code	Species	Li/Ca	Mg/Ca	Li/Mg	Sr/Ca	Li/Mg-derived	$T_{rec} - T_{in-situ}$
		($\mu\text{mol/mol}$)	(mmol/mol)	(mmol/mol)	(mmol/mol)	T ($^{\circ}\text{C}$)	($^{\circ}\text{C}$)
Tara P I7S1c1	<i>Porites</i> sp.	6.13	4.73	1.30	8.93	29.2	1.4
Tara P I7S3c2	<i>Porites</i> sp.	5.58	3.77	1.48	8.98	26.5	-1.3
Tara P I8S1c3	<i>Porites</i> sp.	5.76	4.43	1.30	8.93	29.1	2.0
Tara P I10S0c6	<i>Porites</i> sp.	5.64	4.17	1.35	8.90	28.3	-0.6
Tara P I11S1c7	<i>Porites</i> sp.	6.66	5.30	1.26	8.91	29.8	0.8
Tara P I15S1c10	<i>Porites</i> sp.	5.74	4.88	1.18	8.82	31.1	2.2

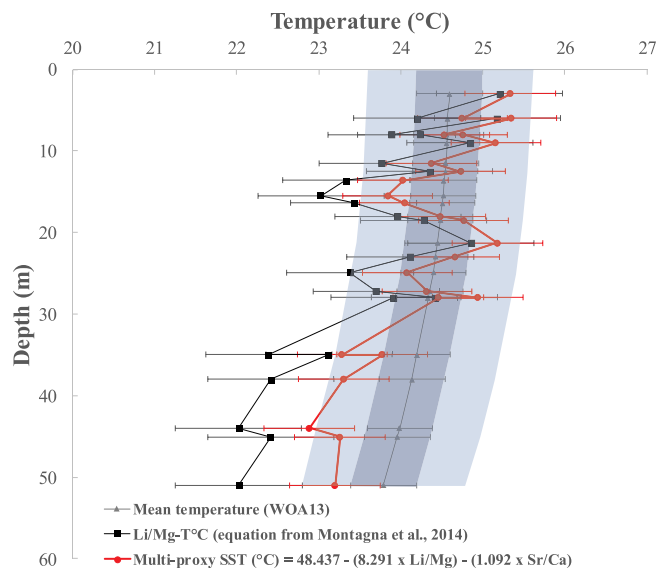


Fig. 4. Depth profile of the ambient mean annual seawater temperature in New Caledonia from WOA13, plotted together with reconstructed temperatures from the Li/Mg exponential equation described by Montagna et al. (2014), and the multi-proxy equation calculated using the Li/Mg and Sr/Ca values from the TARA *Porites* sp. samples (this study). Light and dark blue envelopes represent the seasonal and interannual WOA13 temperature variability, respectively. (For interpretation of the references to colour in this figure legend, the reader is referred to the web version of this article.)

aragonite skeleton without any detectable calcite (Fig. 5).

3.3.2. *Paraconotrochus antarcticus*

The *P. antarcticus* samples show quite different Li/Ca, Mg/Ca and Li/Mg values, with sample GRC-02-014 showing the highest Li/Ca ($19.40 \pm 0.05 \mu\text{mol/mol}$) and Mg/Ca ($7.49 \pm 0.02 \text{mmol/mol}$) and the lowest Li/Mg value ($2.59 \pm 0.08 \text{mmol/mol}$), leading to an excessively warm estimated temperature ($15 \pm 0.9^{\circ}\text{C}$) (Table 2). XRD analysis of this sample revealed the presence of $5.3 \pm 1.0\%$ of Mg-calcite (Fig. 5). 2D mRaman analysis was used to locate the Mg-calcite within the coral skeleton and showed the presence of diagenetic calcite filling a former cavity created by a microborer (Fig. 6). This cavity is 100–150 μm wide and can be few mm long, meandering within the living portion of the coral aragonite (Fig. 6). The LA-ICP-MS analysis of the calcite portion is consistent with high values of Li/Ca ($70.83 \pm 39.15 \mu\text{mol/mol}$) and Mg/Ca ($67.08 \pm 42.47 \text{mmol/mol}$), resulting in low Li/Mg ($1.06 \pm 0.24 \text{mmol/mol}$) and anomalously high Li/Mg-derived temperature ($> 33^{\circ}\text{C}$) (Table S3). The adjacent fibrous aragonite shows much lower values of Li/Ca ($13.19 \pm 3.05 \mu\text{mol/mol}$) and Mg/Ca ($2.68 \pm 0.51 \text{mmol/mol}$) and higher Li/Mg ($4.92 \pm 0.39 \text{mmol/mol}$) that corresponds to a Li/Mg-derived temperature of $1.9 \pm 1.8^{\circ}\text{C}$, closer to the ambient temperature value ($0.93 \pm 0.05^{\circ}\text{C}$).

Two other *P. antarcticus* samples show lower Mg/Ca values, leading to Li/Mg-derived temperatures of 3.6 and $3.8 (\pm 0.9^{\circ}\text{C})$, which are closer to the ambient seawater value, but still overestimated by $\sim 3^{\circ}\text{C}$. XRD analysis of the GRC-02-015 sample revealed the presence of $\sim 0.9\%$ of Mg-calcite.

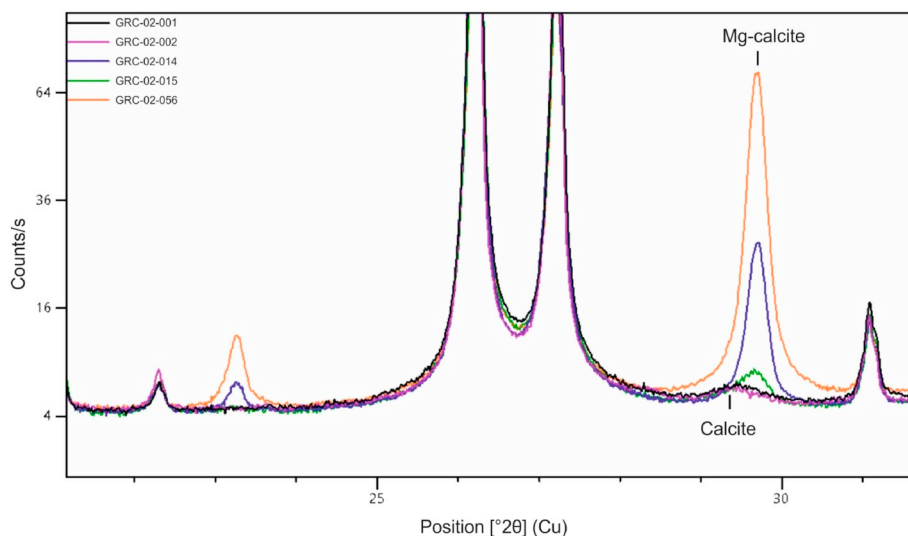


Fig. 5. XRD spectra of the Antarctic samples GRC-02-001, GRC-02-002, GRC-02-014, GRC-02-015 and GRC-02-056. Large high-Mg calcite peaks are observed for samples GRC-02-014, GRC 02-015 and GRC-02-056.

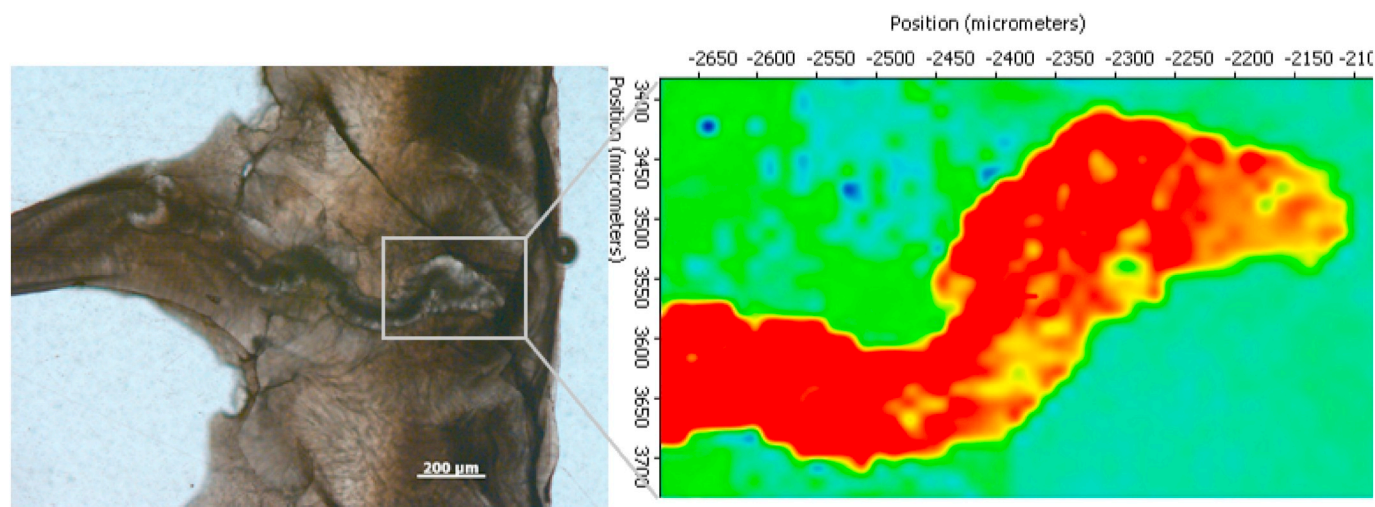


Fig. 6. (left) Cross-section of the thecal wall of the sample GRC-02-014 (*P. antarcticus*), seen under the plane-polarized light. The thecal wall is composed of aragonite fibres radiating in different directions. The micro-structure in the center of the image seems a former cavity created by a microborer that was subsequently filled by diagenetic calcite. (right) 2-D mRaman map of the area delimited by the rectangle. Red and green colours identify pure calcite and aragonite, respectively. (For interpretation of the references to colour in this figure legend, the reader is referred to the web version of this article.)

3.3.3. *F. impensum* and *F. gardineri*

The *F. gardineri* sample GRC-02-056 has anomalously high Li/Ca ($25.04 \pm 0.05 \mu\text{mol/mol}$) and Mg/Ca ($17.45 \pm 0.02 \text{ mmol/mol}$) ratios, resulting in a very low Li/Mg value ($1.43 \pm 0.01 \text{ mmol/mol}$) for cold-water corals from the polar regions (cf. Case et al., 2010; Montagna et al., 2014). The Li/Mg-derived temperature appears to be the most biased, due to the high-Mg/Ca content, resulting in reconstructed temperatures of $27.1 \pm 0.9 \text{ }^\circ\text{C}$, which over-estimates the in situ temperature ($0.93 \pm 0.05 \text{ }^\circ\text{C}$) by $> 26 \text{ }^\circ\text{C}$. Conversely, the *F. impensum* samples GRC-02-002 and CARBONANT34 have Li/Ca values of 12.95 ± 0.07 and $12.70 \pm 0.07 \mu\text{mol/mol}$, and Mg/Ca of 2.59 ± 0.02 and $2.29 \pm 0.02 \text{ mmol/mol}$, resulting in Li/Mg ratios of 5.00 ± 0.01 and $5.55 \pm 0.02 \text{ mmol/mol}$, respectively, which are similar to the value reported by Montagna et al. (2014) ($5.22 \pm 0.06 \text{ mmol/mol}$) for a *F. impensum* specimen collected live from the Balleny islands and growing at $0.75 \text{ }^\circ\text{C}$. Sample GRC-02-056 contains $16.5 \pm 1\%$ of Mg-calcite (Fig. 5), whereas no calcite was detected in the sample GRC-02-002. Similar to the *P. antarcticus* sample GRC-02-014, 2D mRaman analysis showed the presence of diagenetic calcite filling a former cavity. This calcite, analysed by LA-ICP-MS, contains very high values of Li/Ca ($92.23 \pm 13.90 \mu\text{mol/mol}$) and Mg/Ca ($107.86 \pm 5.30 \text{ mmol/mol}$), and very low Li/Mg ($0.85 \pm 0.09 \text{ mmol/mol}$), leading to a high Li/Mg-derived temperature ($> 37 \text{ }^\circ\text{C}$) (Table S3). The values of Li/Ca ($18.85 \pm 1.90 \mu\text{mol/mol}$), Mg/Ca ($3.70 \pm 0.36 \text{ mmol/mol}$), and Li/Mg ($5.09 \pm 0.61 \text{ mmol/mol}$) of the adjacent fibrous aragonite, are similar to those obtained from samples of *J. antarctica* and *P. antarcticus*. The Li/Mg-derived temperature of the fibrous aragonite is $1.2 \pm 2.5 \text{ }^\circ\text{C}$.

3.3.4. *Caryophyllia antarctica*

The *C. antarctica* sample GRC-02-024 shows Li/Ca and Mg/Ca values ($12.98 \pm 0.07 \mu\text{mol/mol}$, $2.65 \pm 0.02 \text{ mmol/mol}$) that are higher than those obtained from sample GRC-02-003 of the same species ($9.95 \pm 0.07 \mu\text{mol/mol}$; $2.00 \pm 0.02 \text{ mmol/mol}$). The Li/Mg ratio is similar in both samples (4.89 and $4.98 \pm 0.02 \text{ mmol/mol}$) yielding reconstructed temperatures that are very close to the ambient seawater value.

3.3.5. *Madrepora oculata*

The element/Ca ratios of the *M. oculata* sample from the Mediterranean Sea are reported as the average $\pm 1\sigma$ SD of 6 different aliquots sub-sampled from the same polyp (Table 2). The Li/Ca, Mg/Ca

and Li/Mg values are $10.72 \pm 0.10 \mu\text{mol/mol}$, $3.81 \pm 0.09 \text{ mmol/mol}$ and $2.82 \pm 0.05 \text{ mmol/mol}$, respectively, with a Li/Mg-derived temperature being only $0.4 \text{ }^\circ\text{C}$ different from the in situ value.

4. Discussion

4.1. Effects of the organic matrix on the coral geochemistry

Most of the *Orbicella* samples collected live from the Mexican Caribbean revealed distinct 2–5 mm thick green bands (Fig. 3), related to the presence of the endolithic green algae *Ostreobium* (Tribollet, 2008; Quiroga Garcia, 2014; Massé et al., 2018). The analyses of coral sub-samples containing the green bands show high levels of Mg/Ca, associated with relatively stable Li/Ca, leading to unusually low Li/Mg values for tropical corals (e.g. 0.59 mmol/mol for MEX 13 compared to $\sim 1.5 \text{ mmol/mol}$ for corals living at similar temperatures; Montagna et al., 2014), and temperatures overestimated by $> 15 \text{ }^\circ\text{C}$ (Table S2). The difference between the Li/Mg-derived temperature and the ambient seawater is mostly attributed to the Mg/Ca ratio (Fig. 7). Conversely, specimens of *P. strigosa* from the same environment are not affected by green bands, and the levels of Mg/Ca and Li/Mg are similar to those for *Porites* spp. (this study; Hathorne et al., 2013; Montagna et al., 2014; D'Olivo et al., 2018; Zinke et al., 2019) and *Siderastrea siderea* (Fowell et al., 2016). Once treated with the oxidative protocol, the *Orbicella* spp. and *P. strigosa* samples show a reduction in Mg/Ca by $> 25\%$ and $\sim 4\%$, respectively, suggesting that Mg is strongly linked to the presence of the green band. In particular, for the *O. faveolata* samples MEX 05 and MEX 13, which are characterized by a very distinct green band (Fig. 3), the Mg/Ca reduction was up to 36%. This value is similar to that reported for *Montastrea faveolata* (now *O. faveolata*) by Watanabe et al. (2001) who suggested that 40% of Mg can be absorbed in organic matter at the surface of the crystals.

Conversely, the chemical treatment did not affect the Li/Ca content, being reduced by only 1% for both genera. This is indicative that the green band is due to the presence of chlorophyll, as the photosynthetic pigment in *Ostreobium* (Jeffrey, 1968) incorporates Mg in its molecular structure. In contrast, the band is not enriched in Li, which is not a chlorophyll component, leading to a significant modification of the initial skeletal Li/Mg ratio. Those results differ from Fowell et al. (2016), who reported a decrease of 25% in Li/Ca due to the removal of organic matter after cleaning with 1% H_2O_2 buffered in 0.1 M NH_4OH . This difference may be explained by a different origin of the organic

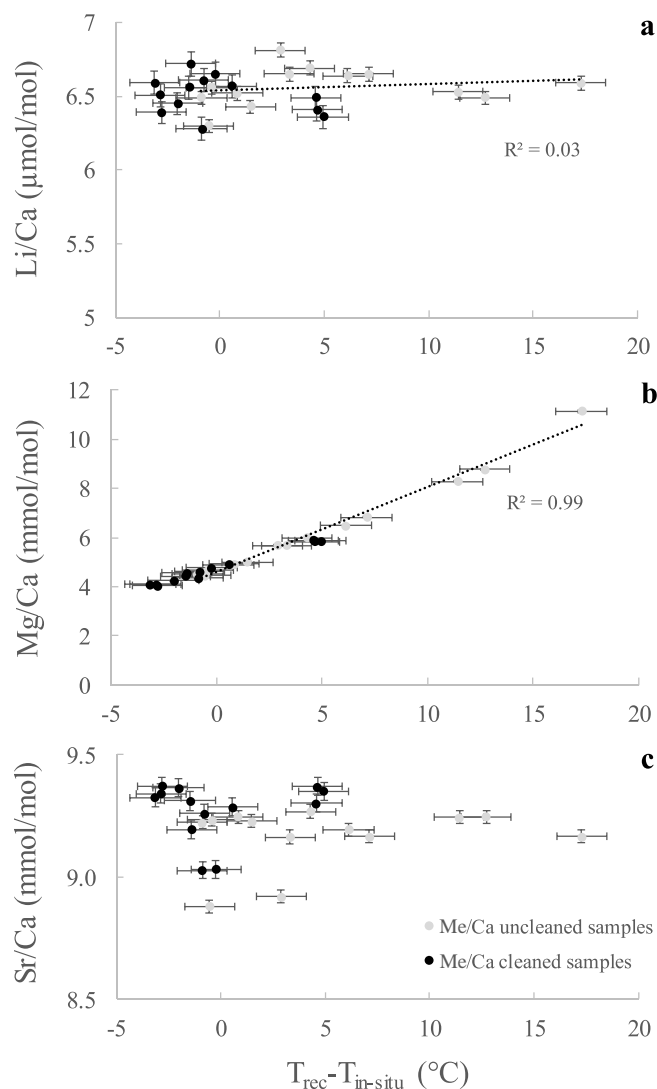


Fig. 7. Li/Ca, Mg/Ca and Sr/Ca values for chemically-treated (black dots) and untreated (grey dots) *Orbicella* spp. samples, plotted against the difference between the reconstructed and instrumental temperature ($T_{\text{rec}} - T_{\text{in-situ}}$). Li/Mg-reconstructed temperatures were calculated using Montagna et al. (2014) equation.

matter, which can be attributed to skeletal tissue in Fowell et al. (2016), and chlorophyll from the *Ostreobium* algae in our study.

Other studies focused on Li/Ca and Li/Mg ratios in corals applied very different cleaning protocols. Case et al. (2010) cleaned the samples (only cold-water corals) using the oxidative and reductive steps of Cheng et al. (2000); Montagna et al. (2014) applied a sequence of oxidative and reductive steps following Lomitschka and Mangini (1999); Hathorne et al. (2013) dissolved samples without any pre-cleaning treatment; Raddatz et al. (2013) used a small quantity of 30% H_2O_2 to clean the skeleton of the cold-water coral *Lophelia pertusa*; and D'Olivo et al. (2018) and Zinke et al. (2019) bleached *Porites* coral slabs in 6% reagent-grade NaClO solution for 24 h.

Overall, our cleaning protocol significantly improved the reconstructed temperatures, reducing the difference with ambient seawater values to $< 3^\circ\text{C}$, except for samples MEX 05 and MEX 13 ($\sim 5^\circ\text{C}$) (Table 2). The incomplete removal of organic matter in those samples strongly marked by green bands could explain this larger shift. Our protocol thus appears to be the most efficient in removing Mg associated with green bands, giving Li/Mg ratios closer to published values for tropical corals. However, reconstructed temperatures can still be up

to 3°C lower than expected for some samples (e.g. MEX 06 and MEX 15) (Table 2), which cannot be easily explained by organic-bound Mg. Part of this difference could be related to the uncertainty of the Li/Mg vs. temperature calibration (Montagna et al., 2014) at the high (tropical) temperatures, but it also reveals a potential species-specific effect regarding the amount of COC-like structures, which is known to be enriched in Mg and can also alter the Li/Mg ratio (Montagna et al., 2014; Rollion-Bard and Blamart, 2015).

The cleaning treatment did not affect the Li/Ca, Mg/Ca and Li/Mg ratios of the *P. lobata* samples from New Caledonia, which is consistent with results from the cleaning test of the M1P-p *Porites* standard (Table S1), suggesting either that the amount of organic matter entrapped in the skeleton of this genus is much less than that present in *O. faveolata*, or the organic component in *Porites* contains little (or no) chlorophyll. Moreover, similar pre- and post-cleaning geochemical values for the New Caledonia samples confirm that our cleaning protocol did not alter the skeletal composition. These results differ somehow from those reported by Montagna et al. (2014) that showed a systematic and comparable % decrease in Li/Ca and Mg/Ca ratios after applying different cleaning steps to the JCp-1 *Porites* standard, all involving a weak acid treatment (i.e. 0.01 and 0.05 N HNO_3). However, the Li/Mg ratio did not change between treated and untreated samples. We speculate that the decrease in Li/Ca and Mg/Ca ratios in Montagna et al. (2014) was due to the weak acid treatment that might have selectively attacked COC and/or fibres.

Overall, our results show a possible species-specific effect. Indeed, despite being collected from the same site, thus implying similar environmental conditions, *Orbicella* spp. and *P. strigosa* differ in relation to the organic matter incorporated, or the nature of this organic component. The genus *Orbicella* seems particularly affected by the organic-bound Mg content, confirming the results of Jones et al. (2015) who obtained high Mg/Ca values (~ 4.6 mmol/mol) for *O. annularis* from the Southern Gulf of Mexico. Conversely, *P. strigosa* and *Porites* appear to be more suitable for paleo-temperature reconstructions based on the Li/Mg proxy.

4.2. Effect of diagenetic calcite on the Li/Mg proxy

Antarctic samples GRC-02-014 (*P. antarcticus*), and GRC-02-056 (*F. gardineri*) show high Mg/Ca values despite being treated with the oxidative cleaning (Table 2). This suggests that the anomalous Mg in these corals is not bound to the organic component oxidized by hydrogen peroxide, and therefore may be associated with calcite. Furthermore, high Mg/Ca values correspond to higher Li/Ca ratios (and relatively lower Sr/Ca), with both ratios showing a strong correlation ($R = 0.85$, $p\text{-value} < 0.001$). A selection of five Antarctic cold-water corals was therefore analysed by X-ray powder diffraction (XRD) and mRaman spectroscopy to identify the presence of carbonate phases other than aragonite. XRD revealed variable amounts of calcite, from 0.9 to 16.5% (Fig. 5), while mRaman allowed precise location of the calcite at micrometer scale within the coral skeleton (Fig. 6). The presence of diagenetic calcite was previously observed in live corals, notably in *Porites* sp. (Lazareth et al., 2016), and is known to bias paleoclimate reconstructions from Sr/Ca or Mg/Ca ratios (McCulloch et al., 1996; McGregor and Gagan, 2003; Nothdurft et al., 2007). However, only a few studies have evaluated the impact of calcite on the Li/Mg ratio. Lazareth et al. (2016) showed that Li/Mg in a *Porites* in Vanuatu has a higher sensitivity to calcite compared to Sr/Ca. These biases are notably due to a considerable enrichment of Mg content in skeleton infilled by diagenetic calcite (Berner, 1975; Allison et al., 2007; Nothdurft et al., 2007; Bryan and Marchitto, 2008; Hathorne et al., 2011; Lazareth et al., 2016). XRD analysis revealed the presence of high-Mg calcite in the skeleton of samples GRC-02-015 (0.9%), GRC-02-014 (5.3%) and GRC-02-056 (16.5%), whereas this carbonate phase was below the detection limit for samples GRC-02-001 and GRC-02-002. Consequently, the Mg/Ca in high-Mg calcite-contaminated samples is much higher than those

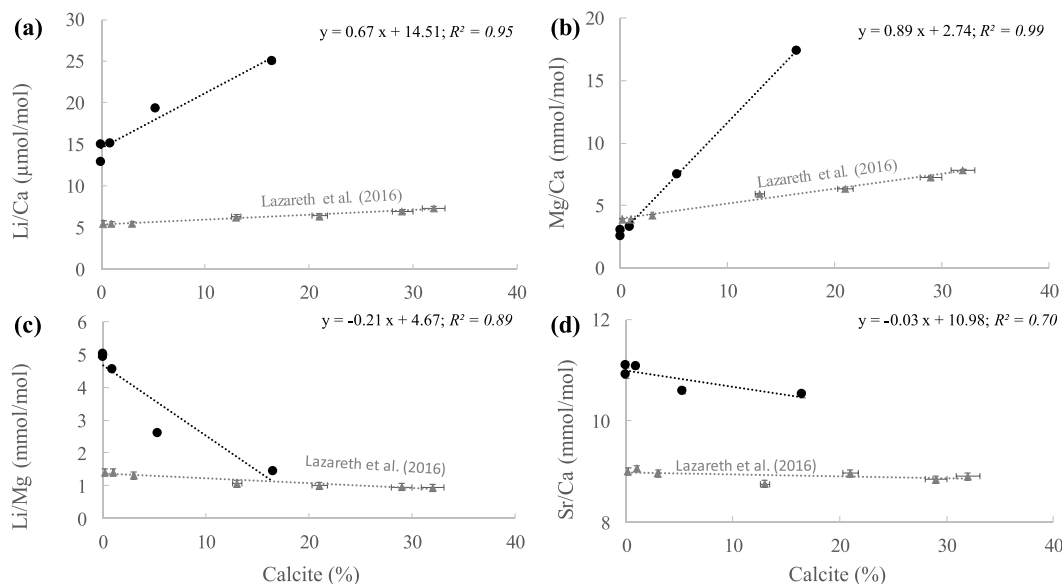


Fig. 8. Variation of Li/Ca, Mg/Ca, Sr/Ca and Li/Mg ratios as a function of high-Mg calcite percentage for the Antarctic samples GRC-02-001, GRC-02-002, GRC-02-014, GRC-02-015 and GRC-02-056. Data from *Porites* sp. Me/Ca vs %Calcite relationships from Lazareth et al. (2016) are shown for comparison.

of pristine samples, which reduces the Li/Mg ratio as previously observed for *Porites* sp. (Lazareth et al., 2016). Li/Mg decreases linearly with the amount of calcite ($R^2 = 0.89$, p -value < 0.001) (Fig. 8c) in response to a steeper increase of Mg/Ca compared to Li/Ca (Fig. 8a, b). Sr/Ca shows a weak decrease with the amount of calcite (Fig. 8d). We can estimate the effect of the Mg-calcite on the different Me/Ca ratios based on the following equations:

$$\text{Li/Ca } (\mu\text{mol/mol}) = 0.67 (\pm 0.09) \times \% \text{Calcite} + 14.51 (\pm 0.70) \quad (1)$$

$$(R^2 = 0.95, p\text{-value} < 0.001)$$

$$\text{Mg/Ca (mmol/mol)} = 0.89 (\pm 0.02) \times \% \text{Calcite} + 2.74 (\pm 0.13) \quad (2)$$

$$(R^2 = 0.99, p\text{-value} < 0.001)$$

$$\text{Sr/Ca (mmol/mol)} = -0.03 (\pm 0.01) \times \% \text{Calcite} + 10.98 (\pm 0.09) \quad (3)$$

$$(R^2 = 0.70, p\text{-value} < 0.04)$$

$$\text{Li/Mg (mmol/mol)} = -0.21 (\pm 0.04) \times \% \text{Calcite} + 4.67 (\pm 0.34) \quad (4)$$

$$(R^2 = 0.89, p\text{-value} < 0.001)$$

Mg/Ca and Li/Ca increase by 0.89 mmol/mol and 0.67 $\mu\text{mol/mol}/\%$ calcite respectively, leading to a decrease in Li/Mg of 0.21 mmol/mol/% calcite, which corresponds to a Li/Mg-derived temperature sensitivity of $\sim +1.5^\circ\text{C}/\%$ calcite for the Antarctic cold-water coral samples (Fig. 9). This is much higher than the temperature sensitivity estimated for the *Porites* sp. in Lazareth et al. (2016) ($+0.27^\circ\text{C}/\%$ calcite; Fig. 9). This difference is likely related to a different composition of the calcite at both sites (e.g. high-Mg vs. low-Mg calcite), precipitated under very different environmental conditions, but further analyses are needed to support this hypothesis. The Sr/Ca ratio is less impacted by the presence of diagenetic calcite, as observed in Lazareth et al. (2016), showing a slight decrease of 0.03 mmol/mol/% calcite.

Taking advantage of such strong linear correlations between Li/Ca

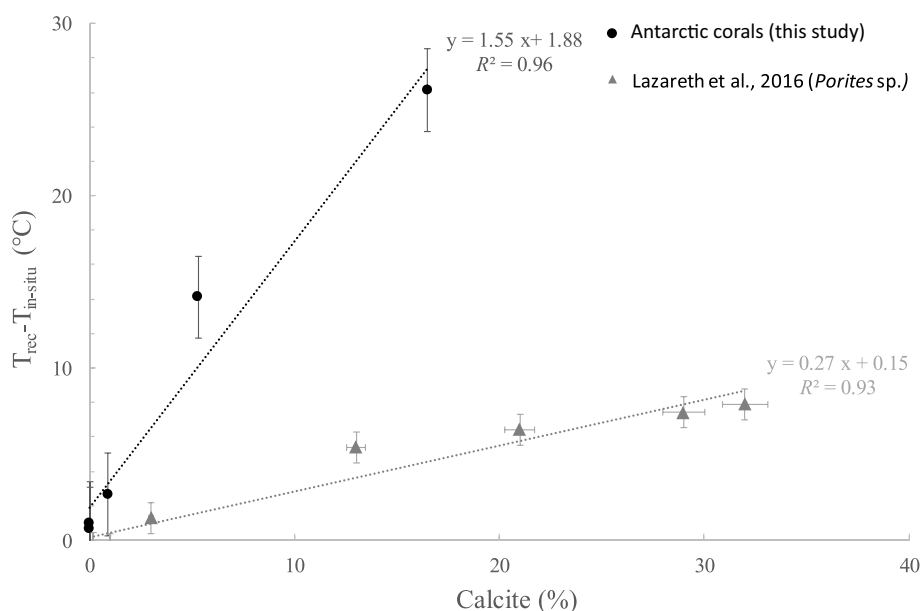


Fig. 9. Difference between the reconstructed and instrumental temperature ($T_{\text{rec}} - T_{\text{in-situ}}$) as a function of the percentage of high-Mg calcite in Antarctic corals (this study) and *Porites* sp. (Lazareth et al., 2016). Li/Mg-reconstructed temperatures were calculated using Montagna et al. (2014) equation.

and Mg/Ca with % of calcite ($R^2 = 0.95$ and 0.99 , respectively) (Fig. 8), corrections were applied to Li/Mg ratios based on the presence of calcite. This correction is based on the assumption that calcite is the only source of anomalous Mg and Li. By normalizing the two intercepts of Li/Ca and Mg/Ca at 0% of calcite (14.51 ± 0.70 $\mu\text{mol/mol}$ and 2.74 ± 0.13 mmol/mol , respectively), a Li/Mg_(0% calcite) ratio of 5.30 ± 0.51 mmol/mol is obtained. This corresponds to a reconstructed temperature of 0.4 ± 2.1 °C, which is similar to the ambient seawater temperature of 0.9 °C. The difference between the Li/Mg-derived temperature and the ambient seawater temperature for the sample showing the highest calcite value (GRC-02-056; 16.5%) is thus significantly reduced, from 26.2 ± 2.4 °C to 0.5 ± 2.1 °C. Similar calculations for *Porites* sp. from Vanuatu provide average corrected temperatures of 27.8 ± 2.1 °C (1σ SD, $n = 7$), which is consistent with in situ annual mean value of 27.9 ± 0.5 °C (Lazareth et al., 2016; Fig. 10).

Although the calcite contribution on the Li/Mg proxy can be reasonably corrected based on a linear regression model, it is important to note that regression coefficients might depend on a series of different factors, including the Mg content of the infilling calcite (i.e. high-Mg vs. low-Mg calcite), and specific regression lines need to be derived for each case study, making this approach problematic. Here, we emphasise the limitations of the Li/Mg-temperature proxy when utilising both live and fossil coral samples that contain traces of diagenetic calcite and suggest possible solutions rather than attempt to provide robust ‘universal’ equations. This approach might be employed when working with particularly valuable samples, such as the Antarctic aragonite cold-water corals, rather than discarding samples with detectable calcite. As calcite within the aragonite skeleton can be located using both mRaman and optical microscopy (Fig. 6), high resolution analysis using laser ablation ICP-MS can be adopted to target pristine aragonite and hence avoid calcite contamination. We focused the laser beam on both the fibrous aragonite and the calcite vein of two Antarctic corals (*F. gardineri* GRC-02-056 and *P. antarcticus* GRC-02-014) (Fig. 6). The Li/Ca and Mg/Ca values of the calcite vein are much higher than those in the fibrous aragonite (Table S3), and are consistent with values obtained by extrapolating the linear regressions for Li/Ca (Eq. (1)) and Mg/Ca (Eq. (2)) to 100% calcite (81.51 ± 9.7 $\mu\text{mol/mol}$ and 91.74 ± 2.13 mmol/mol , respectively). The Li/Mg-derived temperature is ~ 1.5 °C for the aragonite portion and ~ 35 °C for the calcite vein (Fig. 10, Table S3). This value is close to the Li/Mg-derived temperature using the linear regression extrapolated to 100% of calcite (~ 37 °C). Although, laser ablation micro-scale analysis of corals contaminated by calcite appears

as a promising method to reconstruct reliable temperature by targeting only pristine aragonite portions, it would not necessarily avoid the issue of organic contaminants. An effective strategy might be to chemically clean coral slabs before analysing the pristine aragonite portions by laser ablation (see D’Olivo et al., 2018). This approach should be tested in the future to assess whether the organic-bound Mg content is totally removed before laser analysis.

4.3. Depth and light conditions

The 25 *P. lobata* samples collected in New Caledonia along a depth gradient (from 3 to 51 m) were studied in order to investigate the potential effect of depth and light exposure on proxies as recently proposed (e.g. Reynaud et al., 2007; Dissard et al., 2012; Thil et al., 2016). The Li/Mg ratios of these samples do not appear to be affected neither by organic matter nor by the presence of calcite. The Li/Mg-derived temperature, based on the general equation of Montagna et al. (2014), shows an average value of 23.7 ± 0.9 °C (1σ SD, $n = 25$) that matches well the ambient seawater temperature (24.4 ± 0.2 °C, average ± 1 SD of the first 51 m of the water column) (Fig. 4), with a coherent signal of decreasing temperature with depth. Although the Li/Mg-derived temperature shows accurate values compared to ambient seawater for the upper 28 m, with a moderate offset of -0.4 ± 0.6 °C relative to WOA13 v2 temperatures, reconstructed temperatures differ below 35 m, with a greater temperature offset of -1.6 ± 0.6 °C between 35 and 51 m (Table 2, Fig. 4). This underestimation of reconstructed temperature with depth may be attributed to the decrease of light availability along the water column. Impact of light on coral proxies (e.g. Sr/Ca, B/Ca, $\delta^{18}\text{O}$, $\delta^{11}\text{B}$) has been highlighted previously (e.g. Cohen et al., 2001; Reynaud et al., 2007; Dissard et al., 2012; Juillet-Leclerc et al., 2014; Thil et al., 2016; Juillet-Leclerc et al., 2018), but its effect on Li/Mg proxy is still to be documented.

To confirm the potential effect of light on Li/Mg accuracy, some *Porites* colonies were collected at various depths (6, 8, 11.5, 15.5 and 28 m; Table 2) under permanent shady conditions. Reconstructed temperatures from these colonies tend to slightly underestimate the ambient values, with a mean shift of -0.8 ± 0.5 °C ($n = 4$) for the upper water column (3–15.5 m) and larger underestimation observed for *Porites* at 15.5 m (-1.5 ± 0.6 °C). Such temperature difference is comparable to the values calculated from samples growing in deeper water (35–51 m). Shallow-water samples (3–15.5 m) exposed to direct sunlight show negligible temperature difference (0.0 ± 0.7 °C) ($n = 6$). These observations confirm the possible influence of light on the Li/Mg

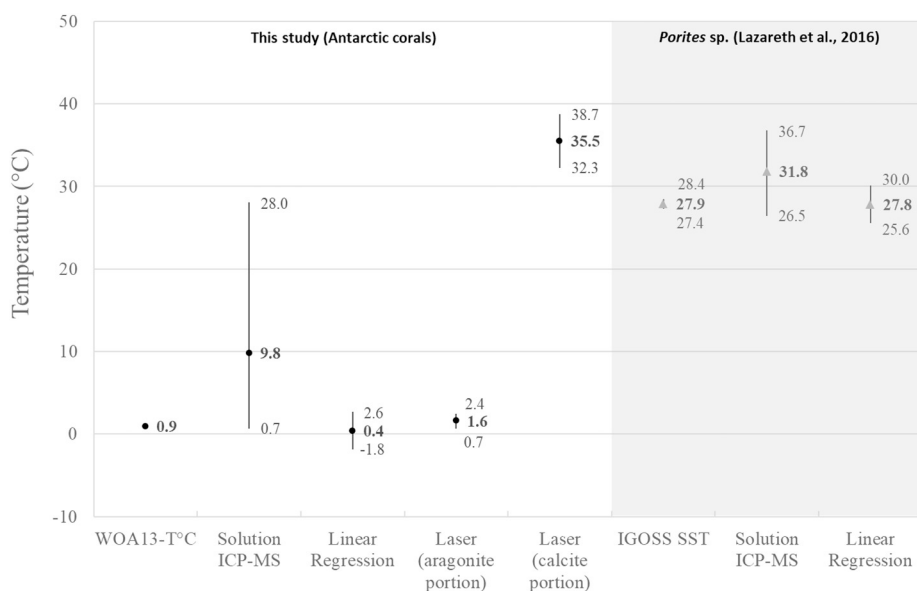


Fig. 10. Ambient and reconstructed temperatures from the Antarctic cold-water corals and *Porites* sp. (Lazareth et al., 2016) affected by diagenetic calcite. Temperatures values were derived from the Li/Mg-T exponential equation reported in Montagna et al. (2014), using the Li/Mg data obtained from the solution-based ICP-MS analysis and the laser ablation ICP-MS analysis of the aragonite and calcite portions, as well as the extrapolated Li/Ca and Mg/Ca values at 0% of calcite (“Linear regression”; see text).

ratio as already observed for other geochemical proxies, thus underestimating temperatures with increasing depth/shady conditions, and may represent a source of uncertainty for paleo-reconstructions from shallow water corals. This needs to be corroborated further with other field data (e.g. corals collected along a depth profile), and/or through culture experiments at different light conditions.

4.4. Refining the Li/Mg calibration and the use of a multi-proxy approach

Most of the existing exponential and linear Li/Mg-temperature calibrations are not well constrained for the very low polar temperatures (< 1 °C), especially owing to the paucity of coral living in extreme sub-freezing conditions (Case et al., 2010; Hathorne et al., 2013; Raddatz et al., 2013; Montagna et al., 2014; Fowell et al., 2016; D'Olivo et al., 2018; Zinke et al., 2019), with the only notable exception being the *F. impensum* specimen analysed by Montagna et al. (2014). New Antarctic samples investigated in the present study represent a unique opportunity to extend the general Li/Mg-temperature equation described by Montagna et al. (2014) to temperatures lower than 1 °C.

A revised exponential regression was obtained by combining the Li/Mg values of all the corals reported in Montagna et al. (2014) with those from the samples analysed in the present study, excluding the ones showing detectable traces of calcite and green bands to avoid integrating anomalous values in the calculation (Fig. 11). The regression analysis was also limited to the two datasets and excluded other less well constrained literature data to minimize differences in the analytical techniques and uncertainties associated with different sample treatments applied before the analysis (e.g. different cleaning protocols or coral sub-sampling).

The new multi-species exponential regression is:

$$\text{Li/Mg (mmol/mol)} = 5.38 (\pm 0.04) \exp(-0.048 \pm 0.001 \times T) \quad (5)$$

$(R^2 = 0.99, p\text{-value} < 0.001)$

The slope and intercept of the exponential relationship and their respective errors were calculated using a weighted linear regression between seawater temperature and the natural logarithm of Li/Mg values, considering both Li/Mg and temperature uncertainties (Thirumalai et al., 2011).

The revised general exponential regression is identical, within the

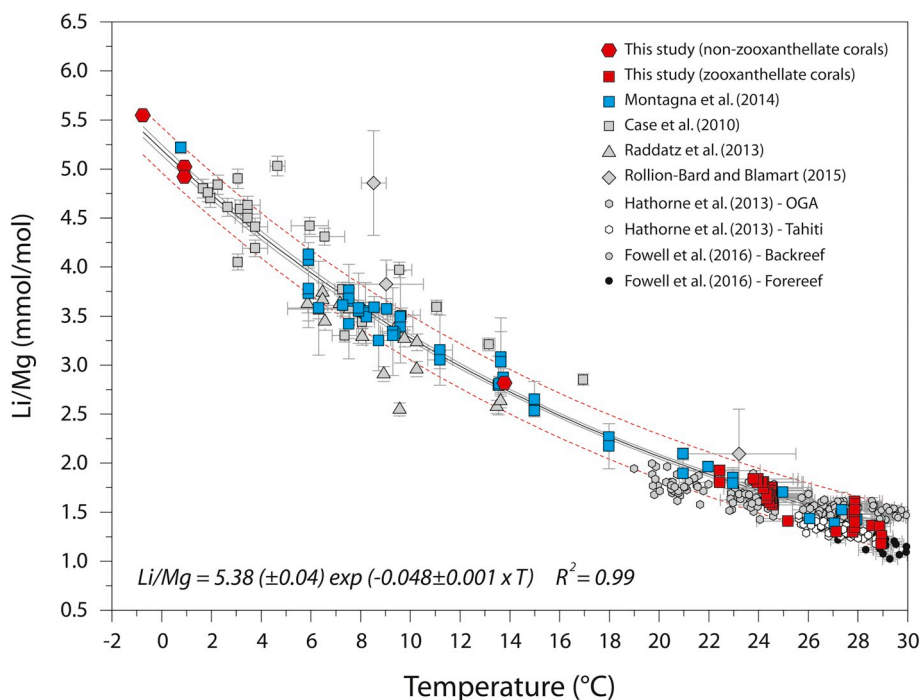


Fig. 11. Li/Mg ratios vs. ambient seawater temperature for the chemically-cleaned zooxanthellate and non-zooxanthellate corals analysed in the present study (red symbols), excluding the samples showing detectable traces of calcite and green bands, plotted together with literature data (Case et al., 2010; Raddatz et al., 2013; Hathorne et al., 2013; Montagna et al., 2014; Rollion-Bard and Blamart, 2015 and Fowell et al., 2016). The grey and red dashed lines show the 95% confidence and prediction intervals, respectively. Local SST values from the OGA and Tahiti coral sites were obtained from the Tokyo Metropolitan Ogasawara Fisheries Center and Gerard (1992), respectively. For further details, refer to Hathorne et al. (2013). (For interpretation of the references to colour in this figure legend, the reader is referred to the web version of this article.)

error, to the equation calculated by Montagna et al. (2014). The overall precision, based on the standard error of estimates, is ± 1.0 °C. If derived from the 95% prediction intervals, the uncertainty of the temperature estimates is ± 0.9 °C at 1 °C, ± 1.5 °C at 12 °C and ± 2.6 °C at 25 °C. Due to the exponential relationship in Eq. (5), the uncertainty becomes larger when the function becomes asymptotic at higher tropical temperatures. Therefore, the application of a general multi-species exponential equation to tropical corals appears to have strong limitations, and linear regression models restricted to the narrow SST range of the tropical species (22–30 °C) maybe more appropriate (Hathorne et al., 2013; Fowell et al., 2016; D'Olivo et al., 2018; Zinke et al., 2019).

Previous studies have highlighted a possible effect of the coral microstructures (COC and fibrous aragonite) on the Li/Mg paleothermometer (Case et al., 2010; Montagna et al., 2014; Rollion-Bard and Blamart, 2015; Marchitto et al., 2018). In particular, COC and fibres have different Li/Mg content, with the COC being generally depleted in Li/Mg compared to the fibres due to a stronger enrichment in Mg compared to Li (Case et al., 2010; Montagna et al., 2014; Marchitto et al., 2018). Similarly, it has been shown that coral Sr/Ca has a microstructure-related pattern, with some studies reporting a preferential Sr/Ca enrichment in COC (e.g. Cohen et al., 2001; Allison et al., 2005) and others showing depleted values (e.g. Shirai et al., 2005) or not much variability between COC and fibres (e.g. Allison et al., 2001; Gagnon et al., 2007). Although these studies used different analytical techniques and investigated different coral species (zooxanthellate and non-zooxanthellate), making results difficult to compare, there do not seem to be a systematic pattern for Sr/Ca in COC vs. fibres. Several hypotheses have been put forward to explain the mechanisms of incorporation of trace elements in COC and fibres and are reviewed in other recent studies (e.g. Rollion-Bard and Blamart, 2015).

Given that Li/Mg and Sr/Ca ratios depend on both temperature and the amount of COC-fibres within the skeleton, they can be combined as a multi-proxy approach to minimize the microstructure effect. Three recent studies have applied a similar approach using Li/Mg and Sr/Ca, or a combination of Sr/Ca, Mg/Ca and Li/Ca to evaluate potential colony specific offsets in SST sensitivity for the tropical corals *Siderastrea siderea* (Fowell et al., 2016) and *Porites* spp. (D'Olivo et al., 2018; Zinke et al., 2019), which showed a slight improvement and a

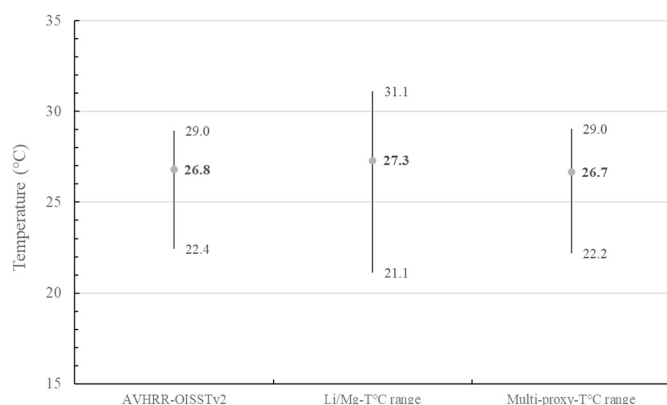


Fig. 12. SST ranges from AVHRR-OISST v2, and reconstructed from the *Porites* sp. samples from the TARA Pacific expedition using the Li/Mg-T exponential equation reported in Montagna et al. (2014), and the Li/Mg – Sr/Ca multi-proxy approach (see text, Eq. (6)). Uncertainties on regressions are ± 1.4 °C and ± 1.03 °C for the Li/Mg and multi-proxy derived temperatures, respectively.

greater confidence in the SST reconstructions compared to individual proxies. Here we have combined Li/Mg and Sr/Ca using the values from the TARA *Porites* sp. samples that span a large temperature range (from ~22 to 29 °C) to obtain the following equation:

$$\text{SST (}^{\circ}\text{C)} = 48.437 (\pm 1.321) - 8.291 (\pm 0.376) \times \text{Li/Mg} - 1.092 (\pm 0.106) \times \text{Sr/Ca} \quad (6)$$

$(R^2 = 0.82, p\text{-value} < 0.001)$

which has a root mean square error of 1.03 °C, which is slightly better than the value of 1.4 °C calculated using the exponential equation by Montagna et al. (2014) on the same samples (Fig. 12). Once applied to the New Caledonia *P. lobata* samples, the multi-proxy equation provides reconstructed temperatures that are closer to the ambient seawater annual mean values, with a root mean square error of 0.6 °C, compared to 1.0 °C using the exponential equation by Montagna et al. (2014) (Fig. 13). This implies that using the combination of Li/Mg and Sr/Ca in *Porites* can effectively reduce the uncertainty of temperature reconstructions and yield values closer to ambient seawater temperatures. However, we did not extend the multi-proxy approach to the entire dataset given the poor sensitivity of Sr/Ca to temperature in cold-water scleractinian corals, with the Sr/Ca ratio being mainly controlled by Rayleigh fractionation processes (Cohen et al., 2006).

4.5. Quality criteria for the Li/Mg proxy

Although we confirm the strong relation of the Li/Mg ratio with seawater temperature based on multi-species exponential calibration from Montagna et al. (2014) (Fig. 11), this study clearly shows that the presence of organic matter, especially that related to endolithic green algae, has a strong effect on the Mg/Ca ratio and hence on the Li/Mg proxy. Thus, organics need to be removed using an oxidative cleaning method as described herein. Furthermore, intra-skeletal calcite deposition in live and fossil corals, even in low concentrations (< 1%), can bias the Li/Mg-reconstructed temperature and needs to be quantified and accounted for. However, given that the error associated with corrections can be large, it is more effective to screen the samples for the presence of calcite by XRD or mRaman. Samples with intra-skeletal calcite can nevertheless be useful to reconstruct paleo-temperatures if the Li/Mg ratios are obtained by laser ablation ICP-MS on pristine fibrous aragonite identified by mRaman.

We have determined criteria that can be useful to assess the quality

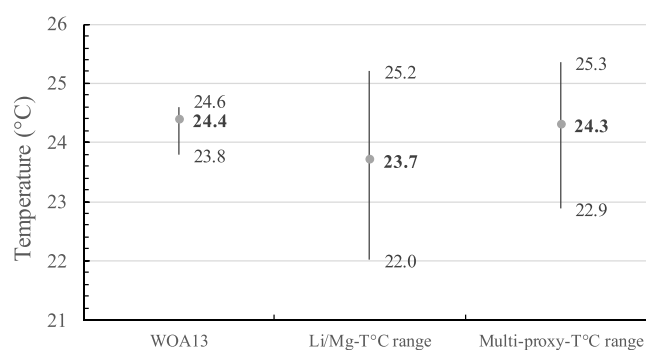


Fig. 13. Ambient and reconstructed temperatures from the *Porites lobata* samples from New Caledonia. Temperature values were derived from the Li/Mg-T exponential equation reported in Montagna et al. (2014), and from the Li/Mg – Sr/Ca multi-proxy approach (see text). Uncertainties on regressions are ± 1.0 °C and ± 0.6 °C for Li/Mg and multi-proxy derived temperatures, respectively.

of the Li/Mg data for paleo-temperature reconstructions: as the Sr/Ca and Li/Mg are both temperature-dependant in shallow-water zooxanthellate corals, they should display a very good correlation ($R = 0.88, p\text{-value} < 0.001$; using data from D'Olivo et al. (2018), Fowell et al. (2016), Hathorne et al. (2013), Raddatz et al. (2013) and Montagna et al. (2014), and the cleaned and calcite-free samples data from this study) (Fig. 14). To first order, the quality of the samples can be evaluated using plots of Sr/Ca versus $\ln(\text{Li/Mg})$ values as shown in Fig. 14. Samples with values outside the 99% prediction bands should be discarded as they would induce a difference between reconstructed and ambient temperatures > 3 °C.

5. Conclusions

This study confirms the strong relationship of aragonite coral Li/Mg with ambient seawater temperature for samples collected live from shallow tropical waters to sub-zero temperatures Antarctic water. However, the reliability of Li/Mg ratios is also affected by the contamination of organic matter within green bands linked to *Ostreobium* algae, and diagenetic calcite within the coral skeleton. Both contaminants are enriched in Mg (and to a lesser degree in Li), leading to unusually low Li/Mg values and hence, to an overestimation of the reconstructed temperature that can be as large as 15–30 °C. We tested different cleaning protocols to remove the green algal band material, with the most effective chemical treatment being a mix of 15% H_2O_2 and 0.5 M NH_4OH . Calcite contamination quantified by XRD can be corrected using the strong linear relationships between Mg/Ca and Li/Ca with the percentage of calcite. However, this requires that XRD must be undertaken on the same powdered samples used for geochemistry, which limits this approach. In contrast, the use of laser ablation ICP-MS together with careful fine-scale observations by optical microscopy or mRaman, can potentially overcome the problem of diagenetic calcite by targeting only pristine aragonite portions.

The revised Li/Mg vs. temperature calibration across contrasting environments, from Antarctic to tropical, yields a regression standard error of ± 1.0 °C. However, owing to the exponential nature of the calibration, large uncertainties are obtained for tropical corals. For these, a multi-linear regression calibration of Li/Mg and Sr/Ca vs. SST shows an identical regression standard error (± 1.0 °C) for *Porites* sp. or better (± 0.6 °C) for *P. lobata* samples from New Caledonia.

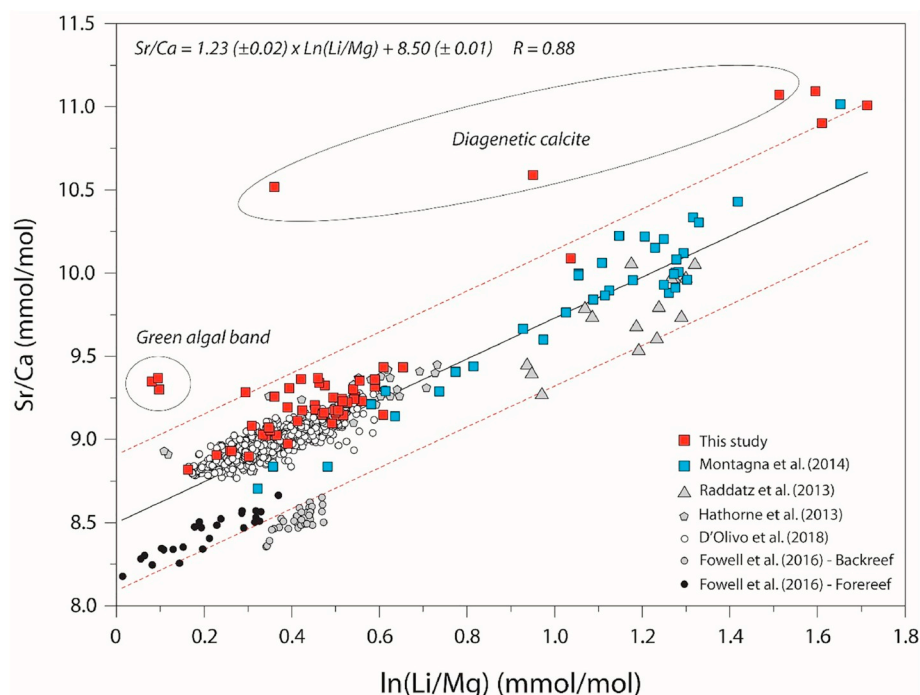


Fig. 14. Paired Sr/Ca vs. ln(Li/Mg) values for all the chemically-cleaned samples analysed in the present study (red squares), plotted together with data from Hathorne et al. (2013) (Sr/Ca values are from Felis et al., 2009), Raddatz et al. (2013), Montagna et al. (2014), Fowell et al. (2016) and D'Oliveo et al. (2018). Linear regression and 99% prediction intervals were calculated using all the available data, excluding the samples with detectable calcite. (For interpretation of the references to colour in this figure legend, the reader is referred to the web version of this article.)

Acknowledgements

This work was supported by the IDI 2016 project funded by the IDEX Paris-Saclay, ANR-11-IDEX-000302. The projects ANR-HAMOC (grant N° ANR-13-BS06-0003-02), INSU COFIMED from the programme MISTRALS-PALEOMEX, PNRA-Geosmart (grant N° PNRA2013/AZ2.06) and PNRA-Graceful (grant N° PNRA16_00069) also contributed to the study. Support by the Posgrado en Ciencias del Mar y Limnología, UNAM, and a Ph. D. fellowship from CONACYT (CVU No. 448526) is acknowledged by SDRE.

Financial support was also received from CONACYT projects CNR C0013-2016-05-277942, SEMARNAT 2016-01-278634 and PDCPN2013-01/214349. Research was also supported by ARC Laureate Fellowship (FL120100049) awarded to MMc, the ARC Centre of Excellence for Coral Reef Studies (CE140100020), and an ARC Future Fellowship (FT160100259) awarded to JAT.

The permit to collect the samples in Puerto Morelos was provided by the Secretaría de Agricultura, Ganadería, Desarrollo Rural, Pesca y Alimentación (SAGARPA, Permiso de Pesca de Fomento No. PPF/DGOPA-042/13). We thank the captains, crews, chief scientists, and scientific parties of the research cruise RECORD and XVII and XXXII Antarctic campaigns. We are keen to thank the commitment of the people and the following institutions for their financial and scientific support that made this singular expedition possible: CNRS, PSL, CSM, EPHE, Genoscope/CEA, Inserm, Université Côte d'Azur, ANR, agnès b., UNESCO-IOC, the Veolia Environment Foundation, Région Bretagne, Serge Ferrari, Billerudkorsnas, Amerisource Bergen Company, Lorient Agglomeration, Oceans by Disney, the Prince Albert II de Monaco Foundation, L'Oréal, Biotherm, France Collectivités, Kankyo Station, Fonds Français pour l'Environnement Mondial (FFEM), Etienne BOURGOIS, the Tara Foundation teams and crew. Tara Pacific would not exist without the continuous support of the participating institutes. Special thanks are due to Guillaume Iwankow for drilling. Thanks are also due to the UMR ENTROPIE (Noumea, New Caledonia) and especially to Fanny Houlbrèque and Claude Payri. We are grateful to Federico Zorzi for the help with the XRD analysis and Anne Juillet-Leclerc for the generous advices on the manuscript. This manuscript benefited from constructive suggestions by three anonymous reviewers. This is LSCE contribution n. 6603, ISMAR-CNR Bologna scientific contribution n. 1978, and publication n. 10 of the Tara Pacific Consortium.

Appendix A. Supplementary data

Supplementary data to this article can be found online at <https://doi.org/10.1016/j.chemgeo.2019.03.038>.

References

- Allen, M.R., Dube, O.P., Solecki, W., Aragón-Durand, F., Cramer, W., Humphreys, S., Kainuma, M., Kala, J., Mahowald, N., Mulugetta, Y., Perez, R., Wairiu, M., Zickfeld, K., 2018; al., in press. Framing and Context. In: Masson-Delmotte, V., Zhai, P., Pörtner, H.-O., Roberts, D., Skea, J., Shukla, P.R., Pirani, A., Moufouma-Okia, W., Péan, C., Pidcock, R., Connors, S., Matthews, J.B.R., Chen, Y., Zhou, X., Gomis, M.L., Lonnoy, E., Maycock, T., Tignor, M., Waterfield, T. (Eds.), *Global Warming of 1.5°C. An IPCC Special Report on the impacts of global warming of 1.5°C above pre-industrial levels and related global greenhouse gas emission pathways, in the context of strengthening the global response to the threat of climate change, sustainable development, and efforts to eradicate poverty*, (In Press).
- Allison, N., 1996. Geochemical anomalies in coral skeletons and their possible implications for palaeoenvironmental analyses. *Mar. Chem.* 55, 367–379.
- Allison, N., Finch, A., Sutton, S., Newville, M., 2001. Strontium heterogeneity and speciation in coral aragonite: implications for the strontium paleothermometer. *Geochim. Cosmochim. Acta* 65 (16), 2669–2676.
- Allison, N., Finch, A.A., Newville, M., Sutton, S.R., 2005. Strontium in coral aragonite: 3. Sr coordination and geochemistry in relation to skeletal architecture. *Geochim. Cosmochim. Acta* 69, 3801–3811.
- Allison, N., Finch, A.A., Webster, J.M., Clague, D.A., 2007. Palaeoenvironmental records from fossil corals: the effects of submarine diagenesis on temperature and climate estimates. *Geochim. Cosmochim. Acta* 71, 4693–4703.
- Amiel, A.J., Friedman, G.M., Miller, D.S., 1973a. Distribution and nature of incorporation of trace elements in modern aragonitic corals. *Sedimentology* 20, 47–64.
- Amiel, A.J., Miller, D.S., Friedman, G.M., 1973b. Incorporation of uranium in modern corals. *Sedimentology* 20, 523–528.
- Banzon, V., Smith, T.M., Liu, C., Hankins, W., 2016. A long-term record of blended satellite and *in situ* sea surface temperature for climate monitoring, modeling and environmental studies. *Open Access* 13.
- Barker, S., Greaves, M., Elderfield, H., 2003. A study of cleaning procedures used for foraminiferal Mg/calcium paleothermometry. *Geochem. Geophys. Geosyst.* 4 (9), 8407.
- Bemis, E.B., Spero, H.J., Bijma, J., Lea, D.W., 1998. Reevaluation of the oxygen isotopic composition of planktonic foraminifera: experimental results and revised paleotemperature equations. *Paleoceanography* 13, 150–160.
- Berner, R.A., 1975. The role of magnesium in the crystal growth of calcite and aragonite from sea water. *Geochim. Cosmochim. Acta* 39, 489–504.
- Boiseau, M., Juillet-Leclerc, A., 1997. H₂O₂ treatment of recent coral aragonite: oxygen and carbon isotopic implications. *Chem. Geol.* 143, 171–180.
- Boyer, T.P., Antonov, J.I., Baranova, O.K., Coleman, C., Garcia, H.E., Grodsky, A., Johnson, D.R., Locarnini, R.A., Mishonov, A.V., O'Brien, T.D., Paver, C.R., Reagan, J.R., Seidov, D., Smolyar, I.V., Zweng, M.M., 2013. *World Ocean Database 2013 (Report)*. NOAA Printing Office.
- Bryan, S.P., Marchitto, T.M., 2008. Mg/Ca-temperature proxy in benthic foraminifera:

- New calibrations from the Florida Straits and a hypothesis regarding Mg/Li. *Paleoceanography* 23, PA2220.
- Case, D.H., Robinson, L.F., Auro, M.E., Gagnon, A.C., 2010. Environmental and biological controls on Mg and Li in deep-sea scleractinian corals. *Earth Planet. Sci. Lett.* 300, 215–225.
- Cheng, H., Adkins, J., Edwards, R.L., Boyle, E.A., 2000. U-Th dating of deep-sea corals. *Geochim. Cosmochim. Acta* 64, 2401–2416.
- Cohen, A.L., Layne, G.D., Hart, S.R., Lobel, P.S., 2001. Kinetic control of skeletal Sr/Ca in a symbiotic coral: Implications for the paleotemperature proxy. *Paleoceanography* 16, 20–26.
- Cohen, A.L., Gaetani, G.A., Lundälv, T., Corliss, B.H., George, R.Y., 2006. Compositional variability in a cold-water scleractinian, *Lophelia pertusa*: New insights into “vital effects”. *Geochem. Geophys. Geosyst.* 7 (12), 12004.
- Corrège, T., 2006. Sea surface temperature and salinity reconstruction from coral geochemical tracers. *Palaeogeogr. Palaeoclimatol. Palaeoecol.* 232, 408–428.
- Cuif, J.P., Dauphin, Y., Farre, B., Nehrke, G., Nouet, J., Salomé, M., 2008. Distribution of sulphated polysaccharides within calcareous biominerals suggests a widely shared two-step crystallization process for the microstructural growth units. *Mineral. Mag.* 72, 233–237.
- DeCarlo, T.M., Ren, H., Farfan, G.A., 2018. The origin and role of organic matrix in coral calcification: insights from comparing coral skeleton and abiogenic aragonite. *Front. Mar. Sci.* 5.
- Dekens, P.S., Lea, D.W., Pak, D.K., Spero, H.J., 2002. Core top calibration of Mg/Ca in tropical foraminifera: refining paleotemperature estimation. *Geochem. Geophys. Geosyst.* 3, 1–29.
- Dissard, D., Douville, E., Reynaud, S., Juillet-Leclerc, A., Montagna, P., Louvat, P., McCulloch, M., 2012. Light and temperature effects on $\delta^{11}\text{B}$ and B/Ca ratios of the zooxanthellate coral *Acropora* sp.: results from culturing experiments. *Biogeosciences* 9, 4589–4605.
- D’Olivo, J.P., Sinclair, D.J., Rankenburg, K., McCulloch, M.T., 2018. A universal multi-trace element calibration for reconstructing sea surface temperatures from long-lived *Porites* corals: removing ‘vital-effects’. *Geochim. Cosmochim. Acta* 239, 109–135.
- Fallon, S.J., Thresher, R.E., Adkins, J., 2014. Age and growth of the cold-water scleractinian *Solenosmilia variabilis* and its reef on SW Pacific seamounts. *Coral Reefs* 33, 31–38.
- Felis, T., Suzuki, A., Kuhnert, H., Dima, M., Lohmann, G., Kawahata, H., 2009. Subtropical coral reveals abrupt early-twentieth-century freshening in the western North Pacific Ocean. *Geology* 37 (6), 527–530.
- Fowell, S.E., Sandford, K., Stewart, J.A., Castillo, K.D., Ries, J.B., Foster, G.L., 2016. Intra-reef variations in Li/Mg and Sr/Ca sea surface temperature proxies in the Caribbean reef-building coral *Siderastrea siderea*. *Paleoceanography* 31, 1315–1329.
- Gagnon, A.C., Adkins, J.F., Fernandez, D.P., Robinson, L.F., 2007. Sr/Ca and Mg/Ca vital effects correlated with skeletal architecture in a scleractinian deep-sea coral and the role of Rayleigh fractionation. *Earth Planet. Sci. Lett.* 261, 280–295.
- García, Quiroga, 2014. Patron de Variación del Crecimiento de las Algas Endolíticas en el Esqueleto del Coral Hermatípico *Orbicella faveolata*. Universidad Nacional Autónoma de México PhD. Thesis.
- Ghosh, P., Adkins, J., Affek, H., Balta, B., Guo, W., Schauble, E.A., Schrag, D., Eiler, J.M., 2006. ^{13}C - ^{18}O bonds in carbonate minerals: a new kind of paleothermometer. *Geochim. Cosmochim. Acta* 70, 1439–1456.
- Hathorne, E.C., Felis, T., James, R.H., Thomas, A., 2011. Laser ablation ICP-MS screening of corals for diagenetically affected areas applied to Tahiti corals from the last deglaciation. *Geochim. Cosmochim. Acta* 75, 1490–1506.
- Hathorne, E.C., Felis, T., Suzuki, A., Kawahata, H., Cabioch, G., 2013. Lithium in the aragonite skeletons of massive *Porites* corals: a new tool to reconstruct tropical sea surface temperatures. *Paleoceanography* 28, 143–152.
- Henry, V.L., Torres, J., 2013. Metabolism of an Antarctic solitary coral, *Flabellum impensum*. *J. Exp. Mar. Biol. Ecol.* 449, 17–21.
- Holcomb, M., DeCarlo, T.M., Schoepf, V., Dissard, D., Tanaka, K., McCulloch, M., 2015. Cleaning and pre-treatment procedures for biogenic and synthetic calcium carbonate powders for determination of elemental and boron isotopic compositions. *Chem. Geol.* 398, 11–21.
- Jeffrey, S.W., 1968. Pigment Composition of *Siphonales* algae in the Brain Coral *Favia*. *Biol. Bull.* 135, 141–148.
- Jones, J.P., Carricart-Ganivet, J.P., Iglesias Prieto, R., Enriquez, S., Ackerson, M., Gabitov, R.I., 2015. Microstructural variation in oxygen isotopes and elemental calcium ratios in the coral skeleton of *Orbicella annularis*. *Chem. Geol.* 419, 192–199.
- Juillet-Leclerc, A., Reynaud, S., Dissard, D., Tisserand, G., Ferrier-Pagès, C., 2014. Light is an active contributor to the vital effects of coral skeleton proxies. *Geochim. Cosmochim. Acta* 140, 671–690.
- Juillet-Leclerc, A., Rollion-Bard, C., Reynaud, S., Ferrier-Pagès, C., 2018. A new paradigm for $\delta^{18}\text{O}$ in coral skeleton oxygen isotope fractionation response to biological kinetic effects. *Chem. Geol.* 483, 131–140.
- Langer, G., Sadekov, A., Thoms, S., Mewes, A., Nehrke, G., Greaves, M., Misra, S., Bijma, J., Elderfield, H., 2015. Li partitioning in the benthic foraminifera *Amphistegina lessonii*. *Geochem. Geophys. Geosyst.* 16, 4275–4279.
- Lazareth, C.E., Soares-Pereira, C., Douville, E., Brahmi, C., Dissard, D., Le Cornec, F., Thil, F., Gonzalez-Roubaud, C., Caquineau, S., Cabioch, G., 2016. Intra-skeletal calcite in a live-collected *Porites* sp.: Impact on environmental proxies and potential formation process. *Geochim. Cosmochim. Acta* 176, 279–294.
- Le Campion-Alsumard, T., Golubic, S., Hutchings, P., 1995. Microbial endoliths in skeletons of live and dead corals: *Porites lobata* (Moorea, French Polynesia). *Mar. Ecol. Prog. Ser.* 117, 149–157.
- Lomitschka, M., Mangini, A., 1999. Precise Th/U-dating of small and heavily coated samples of deep sea corals. *Earth Planet. Sci. Lett.* 170, 391–401.
- Marchitto, T.M., Bryan, S.P., Doss, W., McCulloch, M.T., Montagna, P., 2018. A simple biomineralization model to explain Li, Mg, and Sr incorporation into aragonitic foraminifera and corals. *Earth Planet. Sci. Lett.* 481, 20–29.
- Mass, T., Drake, J.L., Haramaty, L., Kim, J.D., Zelzion, E., Bhattacharya, D., Falkowski, P.G., 2013. Cloning and characterization of four novel coral acid-rich proteins that precipitate carbonates *in vitro*. *Curr. Biol.* 23, 1126–1131.
- Massé, A., Domart-Coulon, I., Golubic, S., Duché, D., Tribollet, A., 2018. Early skeletal colonization of the coral holobiont by the microboring *Ulvophyceae Ostreobium* sp. *Sci. Rep.* 8.
- McCulloch, M., Mortimer, G., Esat, T., Xianhua, L., Pillans, B., Chappell, J., 1996. High resolution windows into early Holocene climate: Sr/Ca coral records from the Huon Peninsula. *Earth Planet. Sci. Lett.* 138, 169–178.
- McGregor, H.V., Gagan, M.K., 2003. Diagenesis and geochemistry of porites corals from Papua New Guinea: Implications for paleoclimate reconstruction. *Geochim. Cosmochim. Acta* 67, 2147–2156.
- Mitsuguchi, T., Matsumoto, E., Abe, O., Uchida, T., Isdale, P.J., 1996. Mg/Ca thermometry in coral skeletons. *Science* 274, 961–963.
- Mitsuguchi, T., Uchida, T., Matsumoto, E., Isdale, P.J., Kawana, T., 2001. Variations in Mg/Ca, Na/Ca, and Sr/Ca ratios of coral skeletons with chemical treatments: implications for carbonate geochemistry. *Geochim. Cosmochim. Acta* 65, 2865–2874.
- Mix, A.C., Morey, A.E., Pisias, N.G., Hostetler, S.W., 1999. Foraminiferal faunal estimates of paleotemperature: circumventing the No-analog problem yields cool Ice Age tropics. *Paleoceanography* 14, 350–359.
- Montagna, P., McCulloch, M., Douville, E., López Correa, M., Trotter, J., Rodolfo-Metalpa, R., Dissard, D., Ferrier-Pagès, C., Frank, N., Freiwald, A., Goldstein, S., Mazzoli, C., Reynaud, S., Rüggeberg, A., Russo, S., Taviani, M., 2014. Li/Mg systematics in scleractinian corals: calibration of the thermometer. *Geochim. Cosmochim. Acta* 132, 288–310.
- Müller, P.J., Kirst, G., Ruhland, G., von Storch, I., Rosell-Melé, A., 1998. Calibration of the alkenone paleotemperature index U_{37}^K based on core-tops from the eastern South Atlantic and the global ocean (60°N–60°S). *Geochim. Cosmochim. Acta* 62, 1757–1772.
- Nothdurft, L.D., Webb, G.E., Bostrom, T., Rintoul, L., 2007. Calcite-filled borings in the most recently deposited skeleton in live-collected *Porites* (Scleractinia): implications for trace element archives. *Geochim. Cosmochim. Acta* 71, 5423–5438.
- Orejas, C., Ferrier-Pagès, C., Reynaud, S., Gori, A., Beraud, E., Tsounis, G., Allemand, D., Gill, J.M., 2011. Long-term growth rates of four Mediterranean cold-water coral species maintained in aquaria. *Mar. Ecol. Prog. Ser.* 429, 57–65.
- Raddatz, J., Liebetrau, V., Rüggeberg, A., Hathorne, E., Krabbenhöft, A., Eisenhauer, A., Böhm, F., Vollstaedt, H., Fietzke, J., López Correa, M., Freiwald, A., Dullo, W.-C., 2013. Stable Sr-isotope, Sr/Ca, Mg/Ca, Li/Ca and Mg/Li ratios in the scleractinian cold-water coral *Lophelia pertusa*. *Chem. Geol.* 352, 143–152.
- Reynaud, S., Ferrier-Pagès, C., Meibom, A., Mostefauji, S., Mortlock, R., Fairbanks, R., Allemand, D., 2007. Light and temperature effects on Sr/Ca and Mg/Ca ratios in the scleractinian coral *Acropora* sp. *Geochim. Cosmochim. Acta* 71, 354–362.
- Reynolds, R.W., Smith, T.M., Liu, C., Chelton, D.B., Casey, K.S., Schlax, M.G., 2007. Daily high-resolution-blended analyses for sea surface temperature. *J. Clim.* 20, 5473–5496.
- Ripple, W.J., Wolf, C., Newsome, T.M., Galetti, M., Alamgir, M., Crist, E., Mahmood, M.I., Lurance, W.F., 2017. World scientists’ warning to humanity: a second notice. *BioScience* 67, 1026–1028.
- Rollion-Bard, C., Blamart, D., 2015. Possible controls on Li, Na, and Mg incorporation into aragonite coral skeletons. *Chem. Geol.* 396, 98–111.
- Sadekov, A., Lloyd, N.S., Misra, S., Trotter, J., D’Olivo, J., McCulloch, M., 2019. Accurate and precise microscale measurements of boron isotope ratios in calcium carbonates using laser ablation multicollector-ICPMS. *J. Anal. At. Spectrom.* 34, 550–560.
- Shirai, K., Kusakabe, M., Nakai, S., Ishii, T., Watanabe, T., Hiyaog, H., Sano, Y., 2005. Deep-sea coral geochemistry: Implication for the vital effect. *Chem. Geol.* 224, 212–222.
- Takeuchi, T., Yamada, L., Shinzato, C., Sawada, H., Satoh, N., 2016. Stepwise evolution of coral biomineralization revealed with genome-wide proteomics and transcriptomics. *PLoS One* 11, e0156424.
- Taviani, M., Angeletti, L., Canese, S., Cannas, R., Cardone, F., Cau, A., Cau, A.B., Follesa, M.C., Marchese, F., Montagna, P., Tassarolo, C., 2017. The ‘Sardinian cold-water coral province’ in the context of the Mediterranean coral ecosystems. *Deep-Sea Res. II Top. Stud. Oceanogr.* 145, 61–78.
- Thil, F., Blamart, D., Assailly, C., Lazareth, C.E., Leblanc, T., Butsher, J., Douville, E., 2016. Development of laser ablation multi-collector inductively coupled plasma mass spectrometry for boron isotopic measurement in marine biocarbonates: new improvements and application to a modern *Porites* coral. *Rapid Commun. Mass Spectrom.* 30, 359–371.
- Thirumalai, K., Singh, A., Ramesh, R., 2011. A MATLABTM Code to Perform Weighted Linear Regression With (Correlated or Uncorrelated) Errors in Bivariate Data 4. *J. Geol. Soc. India* 77 (77), 377–380.
- Tribollet, A., 2008. The boring microflora in modern coral reef ecosystems: a review of its roles. In: Wisshak, M., Tapanila, L. (Eds.), *Current Developments in Bioerosion*. Springer Berlin Heidelberg, Berlin, Heidelberg, pp. 67–94.
- Watanabe, T., Minagawa, M., Oba, T., Winter, A., 2001. Pretreatment of coral aragonite for Mg and Sr analysis: Implications for coral thermometers. *Geochem. J.* 35, 265–269.
- Zinke, J., D’Olivo, J.P., Gey, C.J., McCulloch, M.T., Bruggemann, J.H., Lough, J.M., Guillaume, M.M.M., 2019. Multi-trace-element sea surface temperature coral reconstruction for the southern Mozambique Channel reveals teleconnections with the tropical Atlantic. *Biogeosciences* 16, 695–712.